Diss. 2005 - 13
October

Nuclear Many-Body Continuum States and their Boundary Conditions in a Collective-Coordinate Representation

Resonances and Phase Shifts in Fermionic Molecular Dynamics

Lic. Alberto Cribeiro Santalla

Gesellschaft für Schwerionenforschung mbH
Planckstraße 1 · D-64291 Darmstadt · Germany
Postfach 11 05 52 · D-64220 Darmstadt · Germany

Nuclear Many-Body Continuum States and their Boundary Conditions in a Collective-Coordinate Representation

Resonances and Phase Shifts in Fermionic Molecular Dynamics

Vom Fachbereich Physik
der Technischen Universität Darmstadt

zur Erlangung des Grades
eines Doktors der Naturwissenschaften
(Dr. rer. nat.)

genehmigte Dissertation von

Lic. Alberto Cribeiro Santalla

aus Narón

Darmstadt 2005
D17

Referent:	Prof. Dr. H. Feldmeier
1. Korreferent:	Prof. Dr. R. Roth
2. Korreferent:	Prof. Dr. K. Langanke

Tag der Einreichung:	24.5.2005
Tag der Prüfung:	11.7.2005

All truths are easy to understand once they are discovered;
the point is to discover them.

Galileo Galilei

Contents

Zusammenfassung

Ziel der Kernstrukturtheorie ist es, die vielfältigen Phänomene, die man in Atomkernen und niederenergetischen Kernreaktionen beobachtet, in einem einheitlichen mikroskopischen Modell zu beschreiben. Ausgehend von realistischen Nukleon-Nukleon(NN)-Wechselwirkungen, die die Daten der NN-Streuung und des Deuterons exakt beschreiben, versucht man das quantenmechanische Vielteilchenproblem im ab initio Sinne zu lösen.

In der vorliegenden Arbeit werden in einem mikroskopischen Modell nukleare Resonanzen und Streuphasen elastischer Streuung berechnet. Als Wechselwirkung zwischen den Nukleonen werden sowohl phänomenologische als auch effektive Wechselwirkungen basierend auf realistischen NN-Wechselwirkungen verwendet. Ein Problem solcher mikroskopischer Modelle besteht darin, dass man die asymptotischen ein- und auslaufenden Streuzustände mit Zuständen beschreibt, in denen die Relativbewegung und die intrinsischen Freiheitsgrade der gestreuten Kerne faktorisieren, während man im Wechselwirkungsbereich wegen der Ununterscheidbarkeit der Nukleonen antisymmetrisierte Produkte von Einteilchenzuständen benutzt. Im Raum der total antisymmetrischen Zustände für ununterscheidbare Teilchen kann man jedoch nicht die Nukleonen aus Kern 1 von denen aus Kern 2 unterscheiden, sodass es keinen Operator gibt, der den Abstandsvektor $\vec{r}_{12}$ zwischen Kern 1 und Kern 2 misst. Man hat also keine Darstellung für die Relativkoordinate $\vec{r}_{12}$ wie im asymptotischen Bereich, wo die Antisymmetrisierung der Teilchen zwischen den beiden Kernen keine Rolle mehr spielt.

Aus diesem Grund wird eine Darstellung entwickelt, die es erlaubt, die asymptotischen Streuzustände mit den mikroskopischen Produktzuständen zu verknüpfen. Dazu wird ein Operator $\underset{\sim}{B} = \frac{1}{A}\sum_{i<j}(\underset{\sim}{\vec{x}}(i) - \underset{\sim}{\vec{x}}(j))2$ eingeführt, der symmetrisch bezüglich Teilchenvertauschung ist und die Größe des Systems misst. Seine Eigenzustände in dem verwendeten Vielteilchen-Hilbert-Raum bilden eine Darstellung des Relativabstands, die im asymptotischen Bereich in die gewünschte Faktorisierung relativ-intrinsisch übergeht. Der Winkelanteil der Relativbewegung wird durch explizite Drehimpulsprojektion des Vielteilchensystems berücksichtigt. Solch eine Beschreibung ermöglicht es, die Randbedingungen und die Vielteilchen-Schrödinger-Gleichung in einem modifizierten Eigenwertproblem zusammenzufassen.

Die Darstellung und ihre Anwendung in der Formulierung der Randbedingungen werden zuerst in einem schematischen Modell untersucht. Die Definition eines Abstandsmaßes wird durch den Operator $\underset{\sim}{B}$, der vom relativen Abstand abhängt, in einem beschränkten Hilbertraum realisiert, der von einer diskreten, nicht orthogonalen Basis aufgespannt

wird. Daraus folgt eine diskrete Darstellung bezüglich des relativen Abstandes. Die Eigenvektoren dieses Operators projizieren innerhalb des Hilbertraums auf Zustände mit gut lokalisiertem Abstand, dessen Wert durch den entsprechenden Eigenwert gegeben ist. Die Ableitungen bezüglich des Relativabstands werden durch Potenzen des Kommutators von $\underset{\sim}{B}$ mit dem Hamiltonian erzeugt. Dadurch wird die Formulierung der Randbedingungen durch die Gleichsetzung mehrerer Ableitungen der asymptotischen Coulombwellenfunktionen mit den entsprechenden Ausdrücken der kollektiven Koordinatendarstellung des mikroskopischen Modells ermöglicht.

Zunächst wird die Gültigkeit dieser Methode durch Vergleich mit anderen Methoden gezeigt. Dafür werden dieselben effektiven NN-Wechselwirkungen und Vielteilchenzustände wie bei den anderen Methoden verwendet. Schließlich werden mit dieser Methode Resonanzen und Streuphasen mit einer realistischen Wechselwirkung in einer mikroskopischen, antisymmetrischen Beschreibung des Systems berechnet. Das asymptotische Verhalten von Streulösungen mit ein- und auslaufenden Wellen und von Gamovzuständen mit rein auslaufenden Wellen wird für Systeme mit und ohne Coulombabstoßung untersucht.

Der Vorteil der vorgeschlagenen Methode ist, dass sie keine exakte Faktorisierung von Relativanteil, Winkelabhängigkeit der Relativkoordinate, Schwerpunktsbewegung und den internen Freiheitsgraden der Fragmente erfordert. Außerdem ermöglicht diese Methode eine Verbesserung des Modellraums durch verbesserte Einteilchenzustände und durch Berücksichtigung von Polarisationseffekten in den Vielteilchenkonfigurationen. Die Methode kann auch erweitert werden, um wichtige Probleme in der nuklearen Astrophysik, wie gekoppelte Kanäle („coupled channels") und Kernreaktionen der Art A(a,b)B, behandeln zu können. Eine zusätzliche Eigenschaft der kollektiven Koordinatendarstellung ist die Berechnung effektiver Kern-Kern Potentiale aus der NN-Wechselwirkung.

Introduction

A major goal in low energy nuclear physics is the *ab initio* description of nuclei and nuclear reactions. *Ab initio*, or from the beginning, means in that context, that one regards the nucleons as the fundamental building blocks of nuclei and does not resolve them into quarks or gluons. The nucleons interact via so-called realistic nucleon-nucleon (NN) interactions which reproduce the deuteron properties and the measured phase shifts of nucleon-nucleon elastic scattering. The task is to solve the many-body problem with those realistic interactions, not only for bound states of nuclei but also for resonances and scattering states in the continuum.

Low energy nuclear reactions are of great importance in nuclear astrophysics in order to understand for example the evolution of certain stars and the synthesis of the matter around us. Since not all important reactions are accessible to measurement because they are among short-lived isotopes or at very low energy, it is desirable to develop microscopic models with predictive power.

The general problem which arises in microscopic many-body models is that the asymptotic scattering states consist of two (or more) fragments, each comprising an interacting many-body system. So one has to use a representation that includes the asymptotic states as well as the compound system, in which the clusters overlap strongly or even dissolve. The indistinguishability of the nucleons demands many-body states that are antisymmetric with respect to the exchange of the identical particles. Typically, one represents these as superpositions of Slater determinants, but this is in most cases in contradistinction with the structure of the asymptotic states

$$\left|\,\Psi(k,\ell,J)\right\rangle = \sum_{\substack{m_\ell m_{12}\\ m_1 m_2}} C^{JM_J}_{\ell m_\ell I_{12} m_{12}}\, C^{I_{12}M_{12}}_{I_1 M_1 I_2 M_2}\, \underset{\sim}{\mathcal{A}}\Big(\left|\,\Psi_r(k,\ell,J)\right\rangle \otimes \left|\,\Psi^{I_1 M_1}_{\mathrm{C1}}\right\rangle \otimes \left|\,\Psi^{I_2 M_2}_{\mathrm{C2}}\right\rangle \otimes \left|\,\Psi_{\mathrm{CM}}\right\rangle\Big), \quad (1)$$

which are needed to apply the correct boundary condition to the state $\left|\,\Psi_r(k,\ell,J)\right\rangle$ describing the relative motion. $\left|\,\Psi_{\mathrm{C1}}\right\rangle$ and $\left|\,\Psi_{\mathrm{C2}}\right\rangle$ are the intrinsic states of clusters C1 and C2, respectively, and $\left|\,\Psi_{\mathrm{CM}}\right\rangle$ describes the center of mass motion. $\underset{\sim}{\mathcal{A}}$ is the antisymmetrization operator. For clusters with intrinsic spin zero, $J = \ell$ and all angular momentum resides in the relative motion. For other situations a proper angular momentum projection has to be performed (as is done in Chapter 2).

Such states can be used for nucleus-nucleus scattering or for the breakup of a resonance into two fragments. In the simplest description, the internal degrees of freedom of the

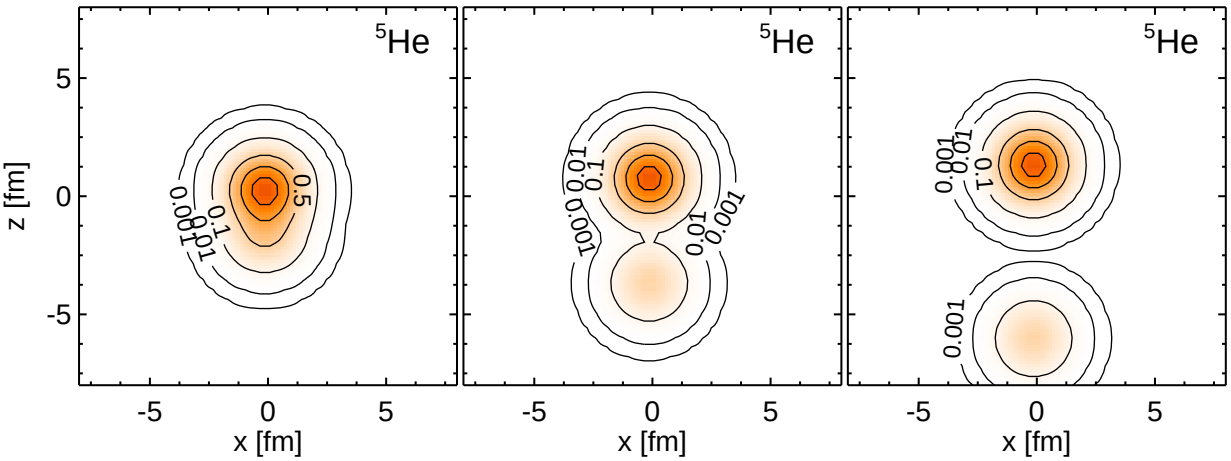

Figure 1: One-body density cuts of ^{5}He in the xz-plane for several n-α separation values (D = 1.5, 4.5 and 7.5 fm from left to right). Contour lines depict density in units of $\rho_0 = 0.16$ fm^{-3}.

fragments are considered frozen, so that the many-body problem

$$\underset{\sim}{H}\big|\,\Psi(k,\ell,J)\,\big\rangle = E\big|\,\Psi(k,\ell,J)\,\big\rangle \tag{2}$$

is reduced to the relative motion

$$\underset{\sim}{H}_r\big|\,\Psi_r(k,\ell,J)\,\big\rangle = E_r\big|\,\Psi_r(k,\ell,J)\,\big\rangle, \tag{3}$$

where E_r is the energy of the relative motion between the clusters.

In the most simplified case, the Hamiltonian $\underset{\sim}{H}_r$ comprises the relative kinetic energy and an effective nucleus-nucleus potential, hence we can regard the system as two internally inert, interacting fragments. The interaction can be obtained from simple approximations like semiclassical methods or by fitting phase shifts and bound state properties. In Chapter 1 we study how to implement the boundary conditions for resonances (Gamov states) and scattering states (phase shifts) in terms of such a schematic model, having in mind the later application to antisymmetrized many-body states, where a relative distance is not an explicit degree of freedom and cannot even be defined as an operator (see Sec. 1.6). Figure (1) illustrates this for ^{5}He. When the neutron and the α-particle are close to each other it is not possible to distinguish the neutron from the other nucleons in the α-particle. The fragments can only be defined asymptotically when the overlap between them is negligible. The states displayed in the figure contribute to the description of n-α scattering states and low-lying n-α resonances to be discussed in Sec. 2.4.2.

In chapter 2 we will use the concepts developed in the microscopic Fermionic Molecular Dynamics (FMD) model and reduce the many-body system, expressed in terms of a superposition of Slater determinants, to a one-dimensional problem in the spirit of a generator coordinate. There will be no nucleus-nucleus potential but rather NN forces based

on realistic NN-interactions, so that the implicit nucleus-nucleus potential originates in the microscopic NN-interactions.

The definition of an appropriate distance measure in terms of a two-body operator acting in the many-body model space, allows us to define in the asymptotic regime, a relative radial wave function for each angular momentum and parity of the many-body system. Using this, the boundary condition specifying that the relative motion is in a Coulomb or free scattering state can be incorporated. The results agree with other methods published in the literature which are not as general.

The application of the collective-coordinate representation to more refined microscopic models, like FMD involving fragments with complex internal structures, will be the subject of future research.

Chapter 1

Schematic Model

In this chapter, we introduce a method to impose general boundary conditions on the Schrödinger equation for the relative motion (3). The general formalism is explained and then applied to two different approaches for the calculation of Gamov, scattering and bound states.

The discussion is then extended to a more general case, in which the Hilbert space of the relative motion is spanned by nonorthogonal basis states that have a certain width in the relative coordinate. In addition, the continuous relative distance operator is replaced by a discrete representation. These steps will help us to construct an operator for the relative distance and to formulate boundary conditions in the microscopic many-body picture of Chapter 2.

1.1 Statement of the problem

The boundary conditions give the additional information needed to determine a unique solution of Eq. (3) with the appropriate behaviour of the system in the incoming and outgoing scattering states. The solution of the Schrödinger equation must match the asymptotic solution outside a chosen boundary $r = R$ in the relative distance. In the region of interest $r \leq R$ we intend to describe the system with our model and in the asymptotic region $r \geq R$ the behaviour of the system is known.

1.1.1 Physical situations and boundary conditions

A boundary condition depends on the physical situation that one intends to describe. A bound system will be restricted to a certain region of space, so the boundary condition will be that the probability density has to go to zero at large distances.

In a collision experiment, the initial state is prepared by an accelerator and a final state is measured, both far away from the interaction region. The boundary conditions must

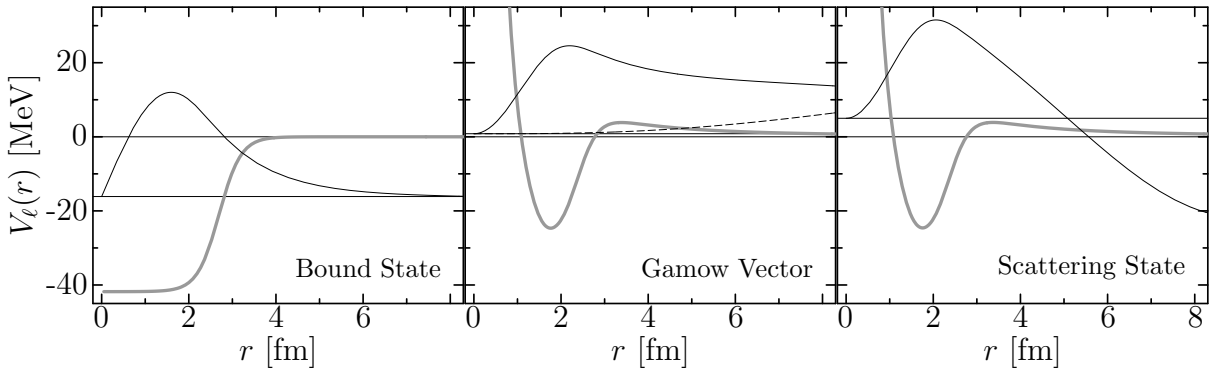

Figure 1.1: From left to right: $\ell = 0,\ J^\pi = 1/2^+$ bound state (Pauli forbidden); $\ell = 1, J^\pi = 3/2^-$ Gamov vector; and $\ell = 1,\ J^\pi = 3/2^-$ scattering state for the ^{4}He+neutron system. The dashed line represents the imaginary part of the Gamov vector, the offsets correspond to the energies of the respective states and the effective energy dependent potential is displayed as a grey line in each case.

be chosen accordingly by matching the interior solution ($r \leq R$) to asymptotic Coulomb states or free spherical waves.

Another case is a system that decays with time. The asymptotic behaviour of this system is described by a purely outgoing wave. This kind of solution, which is called a Gamov state, will be treated in detail in Sec. 1.2.

The schematic representations in Fig. (1.1) show the wave functions for the different physical scenarios considered.

1.1.2 Eigenvalue problem with boundary conditions

Eigenvalue problem in coordinate space

If $\big|\, r \,\big\rangle$ represents the system at a certain relative distance r,

$$\underset{\sim}{r}\big|\, r \,\big\rangle = r\big|\, r \,\big\rangle, \tag{1.1}$$

the trial state is represented by

$$\big|\, \Psi_r(k,\ell,J) \,\big\rangle = \int_0^\infty dr\ \ u_{k\ell J}(r)\ \big|\, r \,\big\rangle \otimes \big|\, (\ell I_{12})JM \,\big\rangle. \tag{1.2}$$

Where $\big|\, (\ell I_{12})JM \,\big\rangle$ denotes its angular-spin part with I_{12} being the total spin of clusters 1 and 2. The amplitude $u_{k\ell J}(r)$ is r times the radial wave function

$$u_{k\ell J}(r) = \big\langle\, r \,\big|\, u(k,\ell,J) \,\big\rangle = r\,\Big(\, \big\langle\, r \,\big|\otimes \big\langle\, (\ell I_{12})JM \,\big|\, \Big)\, \big|\, \Psi_r(k,\ell,J) \,\big\rangle \tag{1.3}$$

which is the solution of the Schrödinger equation in coordinate representation [1]:

$$\underset{\sim}{H}_r \big|\, u(k,\ell,J)\,\big\rangle = \frac{\hbar^2}{2\mu} k_{\ell J}^2 \big|\, u(k,\ell,J)\,\big\rangle \tag{1.4}$$

or

$$\Big(-\frac{\hbar^2}{2\mu}\frac{d^2}{dr^2} + V_\ell(r)\Big)\; u_{k\ell J}(r) = \frac{\hbar^2}{2\mu} k_{\ell J}^2\; u_{k\ell J}(r), \tag{1.5}$$

where

$$V_\ell(r) = U(r) + \frac{\hbar^2}{2\mu}\;\frac{\ell(\ell+1)}{r^2}. \tag{1.6}$$

$V_\ell(r)$ is the effective potential for an angular momentum ℓ and $U(r)$ is the nuclear interaction, plus the Coulomb force if it is required. In some cases $U(r)$ may contain a spin-orbit interaction or depend on ℓ or the energy. μ is the reduced mass of the system.

Formulation of boundary conditions

The boundary condition relates the behaviour of the system described by the wave function $u_{k\ell J}(r)$ with the asymptotic one $w_{k\ell J}(r)$. Since the wave function contains all the information about the system, matching the wave function to the asymptotic solution for $r \geq R$ and to zero at $r = 0$, is sufficient to determine a unique solution. In general the boundary conditions can be expressed as

$$u_{k\ell J}(0) = 0, \tag{1.7}$$

$$u_{k\ell J}(r) = w_{k\ell J}(r), \quad r \geq R. \tag{1.8}$$

$w_{k\ell J}(r)$ is the solution of Eq. (1.5) for $r \geq R$, where $U(r) = 0$.

For a local potential it is sufficient to match the logarithmic derivatives of $u_{k\ell J}(r)$ and $w_{k\ell J}(r)$ at one point R. If the potential depends on the relative momentum higher derivatives may be needed. Alternatively, the interior and asymptotic solution can be matched at several distances. If the coordinate representation $\big|\, r\,\big\rangle$, where the states are exactly localized ($\big\langle\, r \,\big|\, r'\,\big\rangle = \delta(r - r')$), is not used, more than one boundary condition is needed (see Sec. 1.4).

There are two possible types of asymptotic behaviour: free wave, in which one or both fragments have no charge and Coulomb wave, in which both fragments are charged. Depending on the process to be described this can be an outgoing, incoming or scattering wave.

Figure (1.2) illustrates the boundary condition. The right-hand, or outside, region is described by the asymptotic solution corresponding to the centrifugal barrier. The left-hand, or inside, part matches the asymptotic one in a certain region, but once the effective interaction deviates from the centrifugal barrier, the solutions start to differ from each other.

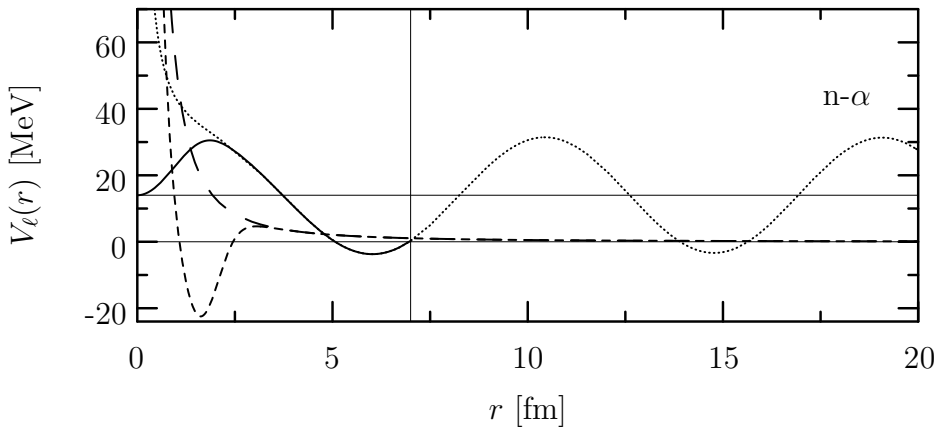

Figure 1.2: Illustration of boundary conditions. Wave function for n-α scattering in $p_{3/2}$ wave with a phenomenological potential (short-dashed line). The solid line shows the solution inside the potential matched to the asymptotic solution (dotted line) that describes a spherical wave with a phase shift. The long-dashed line represents the centrifugal barrier. The vertical line depicts the matching point and the horizontal line marks the energy of the state (14 MeV).

Note that to match the logarithmic derivative the coordinate representation of $\left| \Psi_r(k,\ell,J) \right\rangle$ is needed. Simple or schematic models are usually formulated in coordinate representation, but for a microscopic picture that uses many-body wave functions written in terms of single-particle states, the definition of a distance r between two clusters each consisting of several nucleons is non-trivial. In Sec. (2.2) we shall introduce a macroscopic variable as a measure for the distance.

Modified Eigenvalue Problem

The intention is to implement the boundary condition equations in such a way that we end up with another eigenvalue problem that includes the boundary conditions. To achieve this the boundary conditions are required to be linear and homogeneous in $u_{k\ell J}(r)$ because the eigenvalue equation is. In the following sections this idea is developed for different representations of $\left| \Psi_r(k,\ell,J) \right\rangle$.

1.2 Gamov Vectors

With scattering experiments one can populate resonances which live for a measurable length of time because the system has to tunnel through the nuclear barrier. Resonances are characterized by two parameters: energy and half-life.

Resonances can be treated successfully by means of traditional methods, like S-matrix formalism and phase shift analysis [2]. For our purposes a description in terms of Gamov states [3] is preferred, since we have found that this approach presents several advantages in the framework of microscopic many-body calculations.

A Gamov vector is the state representing a resonance. The difference between this approach and the aforementioned ones, is that it does not consider the formation of the state. S-matrix formalism, or equivalent methods, study the problem of an incoming wave changing to an outgoing spherical one through the scattering process, with the resonance as an intermediate state.

1.2.1 Characterization of a decay process

Let us consider a two-fragment system that forms a resonance. In the simplest approach, the evolution of the system is described by the one-dimensional, time-dependent, Schrödinger equation

$$\big(-\frac{\partial^2}{\partial r^2}+v_\ell(r)\big)u_{k\ell J}(r,t)=i\frac{2\mu}{\hbar}\frac{\partial}{\partial t}u_{k\ell J}(r,t). \tag{1.9}$$

This is the time-dependent version of Eq. (1.5), with $v_\ell(r)=\frac{2\mu}{\hbar^2}V_\ell(r)$. From this, the continuity equation follows:

$$\frac{\hbar}{\mu}\mathrm{Im}\{u^*_{k\ell J}(R,t)\ \frac{\partial u_{k\ell J}}{\partial r}(R,t)\}=-\frac{d}{dt}\int_0^R dr\ |u_{k\ell J}(r,t)|^2. \tag{1.10}$$

The state at $t=0$ is prepared inside the potential well. For example, it can be thought of as an eigenstate with boundary condition

$$u_{k\ell J}(r>R_\ell,t=0)=e^{-kr}, \tag{1.11}$$

where R_ℓ is some point under the barrier and for $r>R_\ell$ the potential is replaced by a constant one to enforce a bound state (see Fig. (1.3)).

For a barrier with a small tunnelling probability the time-dependent solution will become a steady state after a short period of time. The shape of $|u_{k\ell J}(r,t)|$ for $r<R_\ell$ will remain almost unchanged, apart from a slow decrease in its amplitude as a steady flux leaks out. Thus, one can make the following approximate separation ansatz:

$$u_{k\ell J}(r,t)=u_{k\ell J}(r)f_{k\ell J}(t)\ \ \text{for}\ \ r<R, \tag{1.12}$$

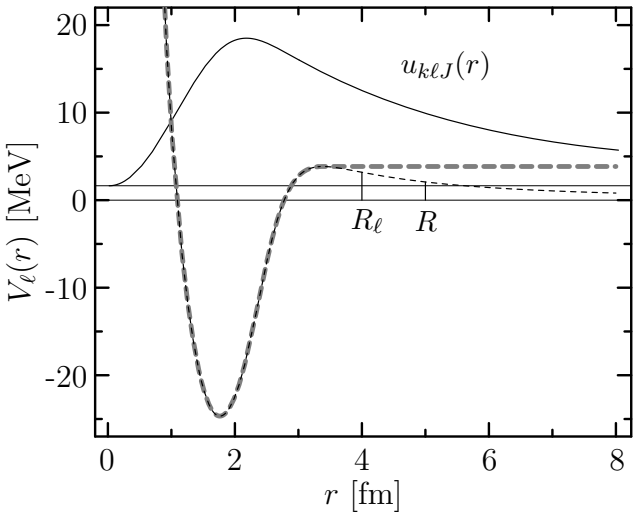

Figure 1.3: The initial condition for a decaying state is shown here for an n-α system in a $p_{3/2}$ wave. The solid line depicts the wave function, the dashed grey line shows the modified potential to enforce an initial bound state and the dashed black line represents the original potential.

that results in the set of equations

$$\Big(-\frac{d^2}{dr^2} + v_\ell(r)\Big) u_{k\ell J}(r) = k_{\ell J}^2 \; u_{k\ell J}(r) \tag{1.13}$$

$$i\frac{2\mu}{\hbar}\frac{df_{k\ell J}}{dt}(t) = k_{\ell J}^2 \; f_{k\ell J}(t), \tag{1.14}$$

where $k_{\ell J}^2$ is a constant. The first equation is an eigenvalue problem with the unknown eigenvalue $k_{\ell J}^2$ and from the second equation follows the time dependence, as

$$f_{k\ell J}(t) = f_{k\ell J}(0) \; e^{-i\frac{\hbar}{2\mu}k_{\ell J}^2 \; t}. \tag{1.15}$$

At a distance R the decay rate $\Gamma_{\ell J}$ can be defined as the quotient of the flux leaking through the surface and the probability of finding the system with a relative distance of less than R:

$$\frac{1}{\hbar}\Gamma_{\ell J} = \frac{\frac{\hbar}{\mu}\,\mathrm{Im}\{u_{k\ell J}(R,t)^* \frac{\partial u_{k\ell J}}{\partial r}(R,t)\}}{\int_0^R dr \; |u_{k\ell J}(r,t)|^2}. \tag{1.16}$$

For small leakage rates this quantity is approximately time-independent.

The ansatz (1.12) inserted in Eq. (1.16) for the decay rate, yields

$$\frac{1}{\hbar}\Gamma_{\ell J} = -\frac{\frac{d}{dt}|f_{k\ell J}(t)|^2}{|f_{k\ell J}(t)|^2} = -\frac{\hbar}{\mu}\,\mathrm{Im}\{k_{\ell J}^2\}. \tag{1.17}$$

Hence, a steady outgoing flux implies a non-vanishing imaginary part of the eigenvalue $k_{\ell J}^2$. Defining a complex energy eigenvalue as

$$z_{\ell J} = \frac{\hbar^2}{2\mu} k_{\ell J}^2 = E_{\ell J} - \frac{i}{2}\Gamma_{\ell J}, \tag{1.18}$$

the decay rate $\Gamma_{\ell J}/\hbar$ is given by the imaginary part of $z_{\ell J}$ and the resonance energy by the real part.

1.2.2 Boundary conditions for the decay

In order to solve the differential equation (1.13) one needs two boundary conditions. The first is $u_{k\ell J}(r = 0) = 0$. The second is given by matching the interior solution for $r < R$ to the exterior one, which is known. Considering the general solution of Eq. (1.5) for $r > R$:

$$w_{k\ell J}(r) = A\ w_{k\ell J}^{\text{in}}(r) + B\ w_{k\ell J}^{\text{out}}(r), \tag{1.19}$$

where $w_{k\ell J}(r)$ is decomposed into incoming and outgoing parts. However, a decaying resonance will have only outgoing components, hence $A = 0$.

The matching distance R has to be taken outside the range of the nuclear interaction, so that $w_{k\ell J}^{\text{out}}(r)$ is the known solution of a scattering problem containing only centrifugal and Coulomb potentials. With these two boundary conditions the Schrödinger equation (1.13) represents a complex eigenvalue problem.

The eigenstate, which is called a Gamov state, fulfills the steady state assumption (1.12) with a steady outgoing flux for $r \geq R$. The real part of the complex eigenvalue is the resonance energy, whilst the imaginary part determines the decay rate, as explained in the previous subsection.

It is important to note that the exterior solution $w_{k\ell J}(r)$ depends on the complex wave number $k_{\ell J} = \sqrt{2\mu z_{\ell J}}/\hbar$ and hence on the as yet unknown eigenvalue $z_{\ell J}$. This implies that an iterative procedure with some initial guess for $k_{\ell J}$ is required.

1.3 Boundary conditions in a grid

The ideas developed in the previous section will be exemplified by a schematic model for calculating resonances and scattering states for the n-α and α-α systems.

1.3.1 One-dimensional grid in coordinate space

The simplest approach to solve Eq. (1.5) under the conditions given in Eq. (1.8), is to discretize the coordinate space into a regular grid in the region $r \in [0, R]$ where the solution is required. Thus the wave function will be given as a list of amplitudes at each position:

$$\begin{aligned} &u_i = u_{k\ell J}(r_i), \quad i = 0, \ldots, n+1, \\ &\Delta = r_i - r_{i-1}, \end{aligned} \tag{1.20}$$

with $r_0 = 0$ and $r_n = R$. Note that we omit the indexes k, l and J in the discretized expressions for simplicity.

Using a three-point formula for the second derivative, the Schrödinger equation (1.5) in this discretized representation reads:

$$-u_{i+1} + (2 + v_i)\, u_i - u_{i-1} = \kappa\, u_i, \quad i = 1, \ldots, n, \tag{1.21}$$

where

$$v_i = \frac{2\mu\Delta^2}{\hbar^2} V_\ell(r_i), \quad \kappa = \Delta^2 \frac{\hbar^2}{2\mu} k_{\ell J}^2. \tag{1.22}$$

This results in n linear equations with $n + 2$ unknowns, $u_0, \ldots, u_{n+1}$. The boundary conditions determine the first and last coefficient. At $r = r_0 = 0$, $u_0 = 0$. At $r = r_n$, the condition given in Eq. (1.8) imposes

$$u_n = w_{k\ell J}(r_n), \quad u_{n+1} = w_{k\ell J}(r_{n+1}), \quad \ldots\ . \tag{1.23}$$

To include this in the eigenvalue problem in such a way that it remains an eigenvalue problem, we need to express these equations as homogeneous and linear in u_i. This can be easily achieved by using the quotient:

$$\frac{u_{n+1}}{u_n} = \frac{w_{k\ell J}(r_{n+1})}{w_{k\ell J}(r_n)} := A_{k\ell J} \quad \text{or} \quad u_{n+1} = A_{k\ell J}\, u_n, \tag{1.24}$$

where $A_{k\ell J}$ is in general a complex number that depends on the complex eigenvalue k and contains the information about the behaviour of the system at the boundary.

Introducing condition (1.24) into Eq. (1.21) for $i = n$, results in a set of n linear

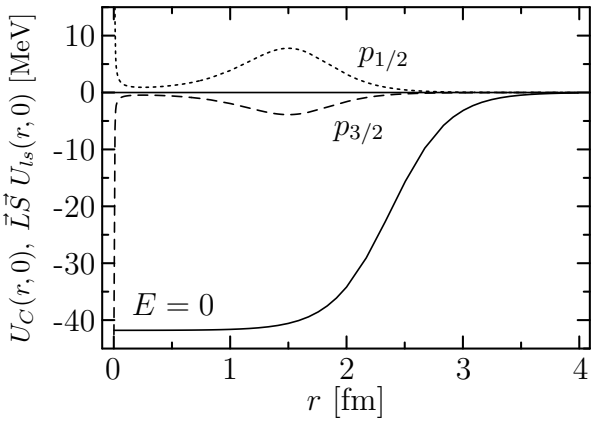

Figure 1.4: Phenomenological n-α potential for neutrons of zero energy from [4]. The solid line depicts the central part. The dashed line represents the $p_{3/2}$ spin-orbit interaction and the dotted line, the $p_{1/2}$.

equations that can be written in matrix form as:

$$\begin{pmatrix} 2+v_1 & -1 & 0 & \dots & 0 \\ -1 & 2+v_2 & -1 & \dots & 0 \\ \vdots & \vdots & \vdots & \ddots & \vdots \\ 0 & \dots & -1 & 2+v_{n-1} & -1 \\ 0 & \dots & 0 & -1 & 2+v_n - A_{k\ell J} \end{pmatrix} \begin{pmatrix} u_1 \\ u_2 \\ u_3 \\ \vdots \\ u_n \end{pmatrix} = \kappa \begin{pmatrix} u_1 \\ u_2 \\ u_3 \\ \vdots \\ u_n \end{pmatrix} . \tag{1.25}$$

The diagonalization of this equation yields the solution with the desired boundary conditions. It is important to point out that in the general case the boundary conditions may depend on the energy of the system, this is the case with resonances and scattering states. Thus, an iterative procedure is needed to solve Eq. (1.25).

Other expressions for the boundary conditions would also be suitable, such as the matching of the logarithmic derivative. Nevertheless the chosen one is the most useful, since the resulting equation is valid for any order in Δ, thus improving the convergence in Δ.

1.3.2 Spherical plane wave

To illustrate a case without the Coulomb interaction we consider the ground state of ^{5}He. The system is modelled on a ^{4}He nucleus in its ground state plus a loosely bound neutron. The only degrees of freedom are the distance between the ^{4}He nucleus and the neutron and the spin of the neutron. The problem can be decomposed into a radial part and a total spin part.

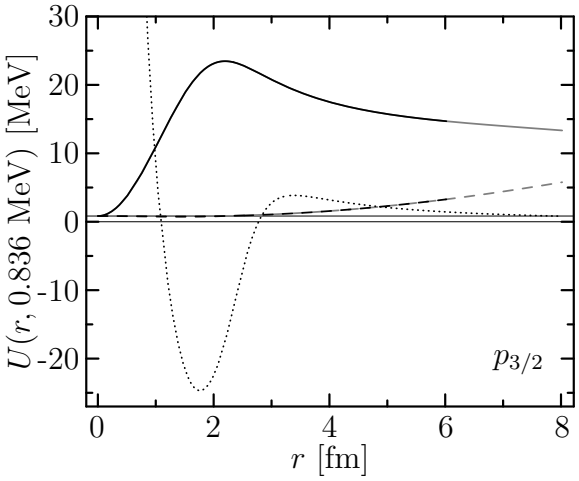

Figure 1.5: Wave function for neutron resonance in grid method for two matching points. The solid lines represent the real part and the dashed lines the imaginary part. Black lines correspond to $R = 6$ fm and grey ones to $R = 8$ fm. Note the exponential increase in the imaginary part.

For the relative motion, G.R. Satchler and L.W. Owen [4] proposed the following spin-dependent potential:

$$U(r,E) = U_C(r,E) + U_{ls}(r,E)\vec{L}\cdot\vec{S} = \frac{-V}{(e^x+1)} + V_s\,\frac{1}{r}\,\frac{d}{dr}\frac{1}{e^{x_s}+1}\;\vec{L}\cdot\vec{S}, \tag{1.26}$$

where

$$\vec{L}\cdot\vec{S} = \frac{1}{2}\Big(J(J+1) - \ell(\ell+1) - \frac{3}{4}\Big), \quad x = \frac{r-R_C}{a}, \quad x_s = \frac{r-R_s}{a}. \tag{1.27}$$

The adjusted parameters that reproduce the experimental phase shifts of ^{5}He are

$$\begin{aligned} V &= 41.8\ \text{MeV} & V_s &= 11.9933\ \text{MeV} + 0.500348E \\ R_C &= (2.3757 - 0.0198\frac{E}{\text{MeV}})\ \text{fm} & R_s &= 1.5838\ \text{fm} \\ a &= 0.25\ \text{fm} \end{aligned} \tag{1.28}$$

and the reduced mass of the system is $\mu = 749.68$ MeV. Note the energy dependence of the parameters V_s and R_C. Since the potential is supposed to be real, we evaluate it with the real part of the energy eigenvalue: $E = \mathrm{Re}\{\hbar^2 k_{\ell J}^2/(2\mu)\}$.

The shape of the potential is shown in Fig. (1.4). The central part and the spin-orbit interaction for $p_{3/2}$ and $p_{1/2}$ are displayed for zero energy.

Since the potential reproduces the phase shifts for the elastic scattering ^{4}He(n,n)^{4}He, it is possible to use it for calculating the resonance behaviour by means of Gamov states or via the phase shifts.

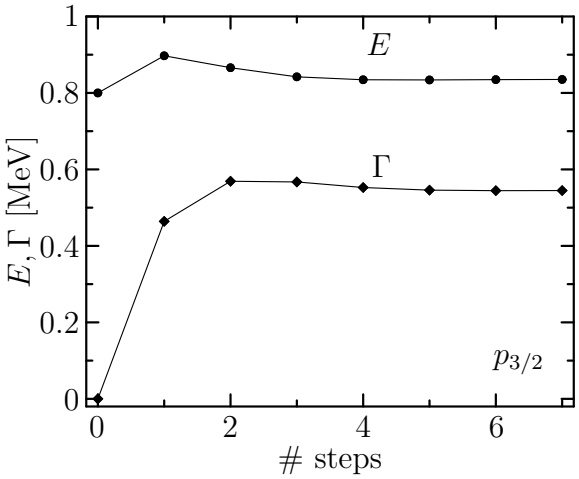

Figure 1.6: The convergence of the eigenvalue plotted against the number of iterations shown using the grid representation for Gamov vectors in the n-α system. Results above are for $R = 8$ fm, $\Delta = 0.02$ fm.

Asymptotics

Since the spin-orbit interaction vanishes for large distances ($r \gtrsim 5$ fm), the asymptotic behaviour is that of free spherical waves, given by Bessel functions. Depending on the state we intend to describe, there are several possibilities:

- scattering state

$$w^{\mathrm{S}}_{k\ell J}(r) = r\,\Big(j_\ell(kr) - \tan\left(\delta_{\ell J}(k)\right)\, n_\ell(kr)\Big), \tag{1.29}$$

- resonance (Gamov vector)

$$w^{\mathrm{G}}_{k\ell J}(r) = r\; h^{(1)}_\ell(kr) = r\;\left(j_\ell(kr) + i n_\ell(kr)\right), \tag{1.30}$$

- bound state

$$w^{\mathrm{B}}_{k\ell J}(r) = e^{-kr}, \tag{1.31}$$

j_ℓ is a spherical Bessel function of the first kind and n_ℓ is one of the second kind. $h^{(1,2)}_\ell$ are Hankel functions, or Bessel functions of the third kind. $h^{(1)}_\ell$ is the purely outgoing wave and $h^{(2)}_\ell$ is the purely incoming one.

The boundary condition (1.31) for a bound state can be imposed in a region outside the range of the potential, where the probability density is not yet zero but exponentially decreasing.

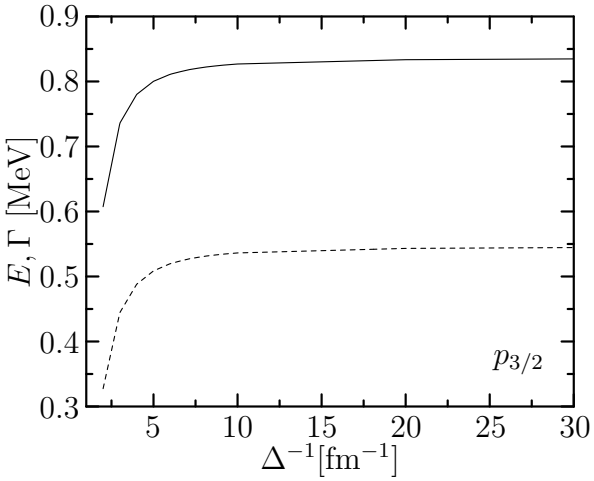

Figure 1.7: The convergence of the eigenvalue plotted against the grid size, shown in the grid representation for the $p_{3/2}$ neutron resonance. $R = 6$ fm.

Results

The n-α system has two neutron resonances at low energy, $p_{3/2}$ and $p_{1/2}$. The chosen potential reproduces the phase shifts of the three channels $s_{1/2}$, $p_{1/2}$ and $p_{3/2}$. For $\ell = 0$, the potential produces a bound state which is forbidden due to the Pauli principle because the α particle has already two neutrons in $s_{1/2}$. Nevertheless, it can be used as a test for the application of the boundary conditions to a bound state. Thus it is possible to apply all the different boundary conditions discussed previously in order to test the method.

Note that the energy dependence of the potential demands an iterative procedure, even for a boundary condition which is independent of the energy.

In the following we show for the $p_{3/2}$ resonance the convergence of the solutions with respect to iterations in the complex energy, the grid spacing $\Delta \to 0$ and the dependence on the matching point R. Using the boundary conditions for scattering or bound states yields similar results.

Figure (1.6) shows that the energy iteration converges within the first few steps, when the initial energy z is put into the potential and the matching condition is taken to be the real eigenvalue for $u_n = 0$. When the boundary conditions are applied at a matching point where the potential $U(r, E)$ is not negligible, oscillations occur, more steps are needed and it converges to an incorrect solution. This effect is independent of the energy dependence of the potential. It gives an indication that the boundary conditions have not been properly applied. This is of little relevance in the present case but might prove helpful in FMD, since there it is not possible to determine the range of the nuclear force so easily.

When the nuclear potential is negligible the solution does not depend on the matching point R. This is depicted in Fig. (1.5) where the wave function is plotted for two matching points. The solutions lie on top of each other and the resulting eigenvalues also coincide.

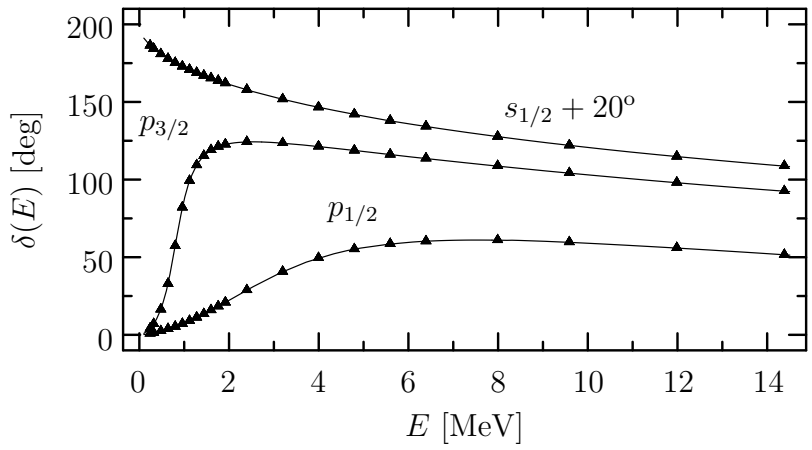

Figure 1.8: Phase shifts for n-α scattering calculated in grid representation. Triangles are from [4], lines are from present work.

In this figure we also see the exponentially increasing imaginary part of the Gamov vector.

Finally Fig. (1.7) shows the convergence as the step size is decreased. A step size of $\Delta = 0.02$ fm is sufficiently small to achieve an accuracy of 1%.

The results for the two p resonances calculated using the Gamov vector boundary condition are listed in table (1.1), the outcome of the phase shift analysis is also shown. This consists of a fit to the integral of a Breit-Wigner function, plus a linear background in the energy range from 0 to 8 MeV for the $p_{1/2}$ resonance and from 0 to 4 MeV for the $p_{3/2}$ resonance, the experimental values are also quoted. Note the difference between Gamov vector and phase shift analysis due to the fact that the width of the resonance is large, $E \approx \Gamma$.

Phase shifts calculated with the boundary condition for scattering states are shown in

	$p_{3/2}$		$p_{1/2}$	
	E [MeV]	Γ [MeV]	E [MeV]	Γ [MeV]
Phase Shift	0.810(2)	0.610(11)	2.26(1)	4.22(6)
Gamov Vector	0.836	0.545	2.92	4.60
Experiment	0.798	0.648	2.07	5.57

Table 1.1: Comparison of resonance parameters for n-α system as determined from phase shift analysis, Gamov Vectors and experimental data [5] (results are shown in the grid representation). Experimental errors are less than 1%.

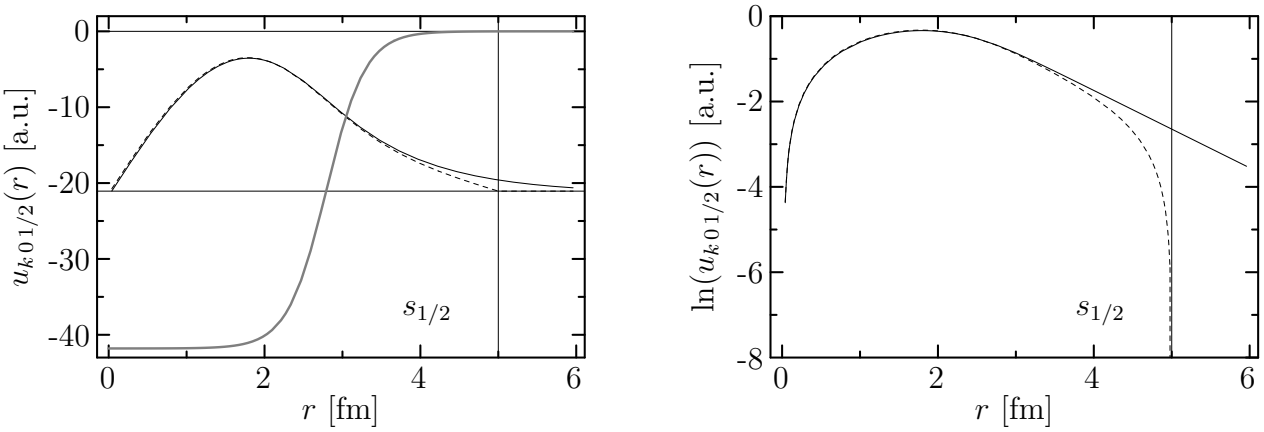

Figure 1.9: Wave function of the Pauli forbidden s-wave bound state for the n-α system in the grid representation. The dashed line represents the boundary condition $u_n = u_{k\,0\,1/2}(R = 5 \text{ fm}) = 0$ and the solid line represents the exponentially decaying condition. A linear scale is used on the left and a logarithmic one on the right. The potential is depicted in grey.

Fig. (1.8). The result agrees with that of Satchler and Owen. The speed

$$SP(E) = \hbar \left| \frac{d\delta}{dE} \right| \tag{1.32}$$

obtained with a numerical derivative, is displayed in Fig. (1.10). The two resonances are visible as peaks, centered at the resonance energy and the FWHM value as the corresponding width. The presence of some background can be deduced from the asymmetry of the contours, which deviate from the typical Breit-Wigner curve.

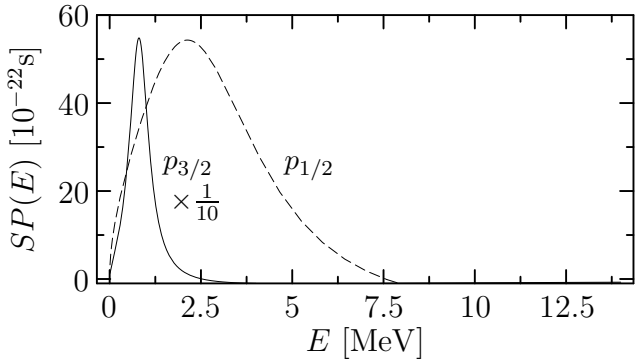

Figure 1.10: Speed plots of calculated phase shifts for n-α resonances in the grid representation. The $p_{3/2}$ amplitude has been reduced by a factor of ten for clarity.

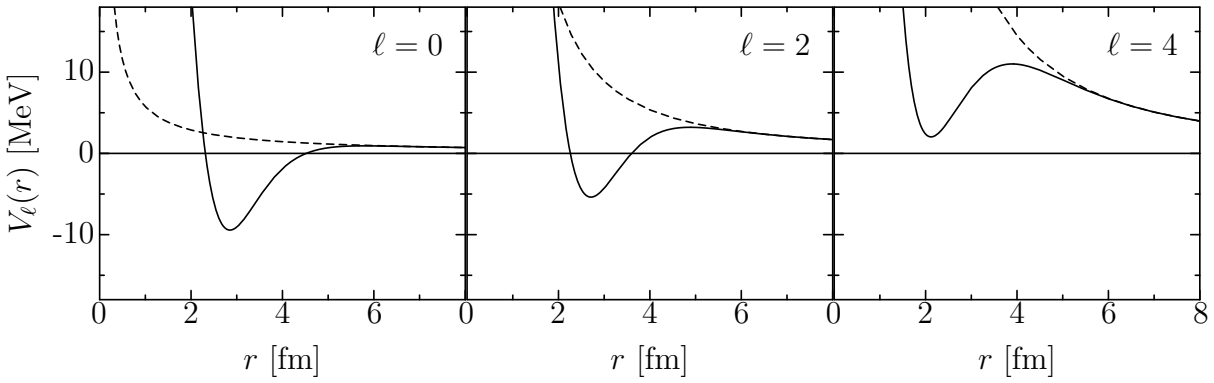

Figure 1.11: The effective potential (consisting of the Ali-Bodmer α-α potential and the Coulomb and centrifugal potential for point-like particles) is depicted for several angular momenta. A dashed line indicates Coulomb plus centrifugal potential alone.

The Pauli forbidden bound state is calculated with the boundary condition (1.31). In Fig. (1.9) the result is compared with the boundary condition $u_n = u_{k\,0\,1/2}(R) = 0$. The logarithmic scale emphasizes the difference between both approaches. Matching the wave function to an exponential tail gives a stable value for the energy that does not depend on the matching point R, as long as it is outside the nuclear potential. Thus, both conditions yield the same result, but (1.31) is computationally more efficient as the accuracy does not depend on R anymore.

1.3.3 Coulomb wave

Now that we tested the validity and accuracy of the method for a free spherical wave, we introduce in and out-going Coulomb waves as asymptotic states. For this we consider ^{8}Be which is known to consist of two interacting ^{4}He nuclei (α-particles), which form a narrow resonance with an angular momentum of zero. If one assumes the α particles to be inert, the only degree of freedom is the distance between the centers of mass of the α particles. The α particles have intrinsic spin zero, so $J = \ell$.

The α-α potential, which reproduces the experimental phase shifts of the α-α scattering, is taken from Ali and Bodmer [6]:

$$U_\ell(r) = V_r(\ell)\; e^{-\mu_r^2\; r^2} - V_a\; e^{-\mu_a^2\; r^2} + 1.44 \text{ MeV fm } \frac{4}{r}. \tag{1.33}$$

The parameters are adjusted to match the phase shifts and the reduced mass of the system is $\mu = 1864.20$ MeV/c^2. An angular momentum dependence in the repulsive part of the potential is allowed for, hence yielding a better fit to the experimental results. The

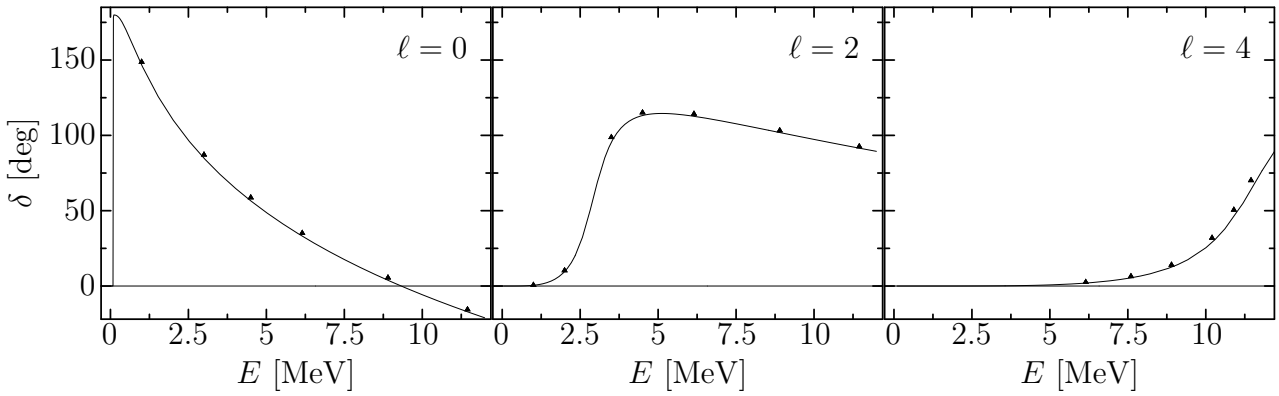

Figure 1.12: Phase shifts for α-α calculated in grid representation. Triangles depict the original calculation of S. Ali and A.R. Bodmer.

parameters are:

$$\begin{aligned} V_a &= 130 \text{ MeV} & \mu_a &= 0.475 \text{ fm} \\ V_r(0) &= 500 \text{ MeV} & & \\ V_r(2) &= 320 \text{ MeV} & \mu_r &= 0.7 \text{ fm} \\ V_r(4) &= 10 \text{ MeV} & & \end{aligned} \tag{1.34}$$

When working with a Hilbert space spanned by gaussians, this potential has the advantage that the matrix elements can be evaluated analytically. The different effective potentials are shown in Fig. (1.11).

Asymptotics

The asymptotic behaviour of the system is given by the Coulomb wave functions, which can be evaluated by means of the method given in [7]. The general solution to the Schrödinger equation for a Coulomb potential is

$$w_{k\ell}(r) = C_1 \; F(kr, \ell) + C_2 \; G(kr, \ell). \tag{1.35}$$

$F(kr, \ell)$ is the regular Coulomb wave function and $G(kr, \ell)$ is the irregular or logarithmic one. For scattering states, the solution is given in [8]):

$$w_{k\ell}(r) = F(kr, \ell) + \tan(\delta_\ell(k)) \; G(kr, \ell). \tag{1.36}$$

The purely outgoing solution is

$$w_{k\ell}(r) = iF(kr, \ell) + G(kr, \ell). \tag{1.37}$$

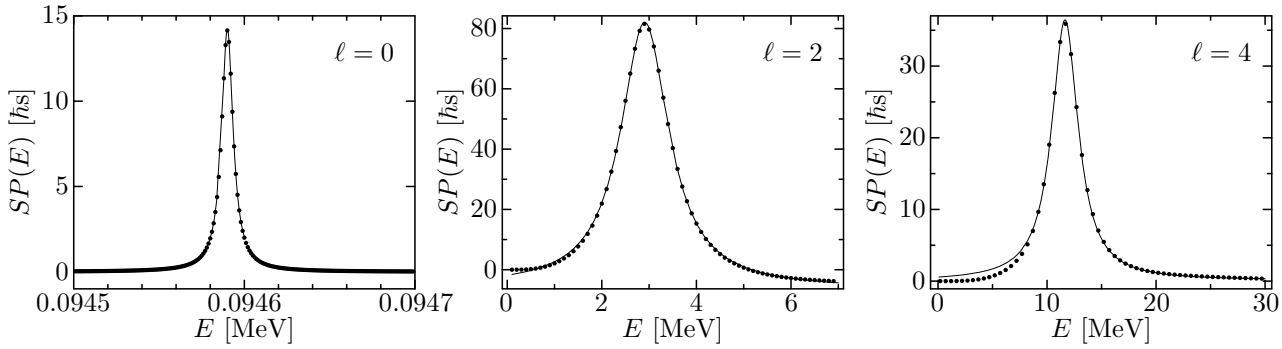

Figure 1.13: Speed plots for an α-α system in the grid representation. The dots represent the calculated points and the lines show the best fit to the resonance.

Results

Resonance energies and widths are calculated for the various angular momenta, since the interaction reproduces the phase shifts for these partial waves at low energy. The results, together with the ones obtained from phase shift analysis, are displayed in Table (1.2).

Resonances for $\ell = 0$ and 4 are good candidates for a Gamov vector approximation, since $\Gamma/E \ll 1$ (see Sec. 1.2). Although the phase shifts are not fitted for the whole region where the resonances occur, the results agree fairly well with the experimental ones. The width and energy of the resonance for $\ell = 2$ are of the same order of magnitude, consequently the Gamov vector approach differs somewhat from the experimental one.

The phase shift analysis yields similar results although the uncertainty is higher, since a certain background is needed for the fit. The quoted figures for $\ell = 2$ were obtained with a quadratic polynomial for the background in the phase shifts, by fitting in the energy range up to 6 MeV. For $\ell = 4$, a quadratic polynomial again provides the best fit to the results up to 25 MeV. $\ell = 0$ can be fitted without a background because the width of

	$\ell = 0$		$\ell = 2$		$\ell = 4$	
	E [MeV]	Γ [eV]	E [MeV]	Γ [MeV]	E [MeV]	Γ [MeV]
Phase Shift	0.0946	7.93	2.91(1)	1.23(1)	11.7(1)	3.03(2)
Gamov Vector	0.0946	7.93	2.90	1.28	11.6	3.11
Experiment	0.09204(5)	5.57(25)	3.12(1)	1.513(15)	11.44(15)	≈3.5

Table 1.2: Comparison of resonance parameters for an α-α system, as determined in the grid representation (see Table (1.1)). Also shown are the experimental results taken from [9].

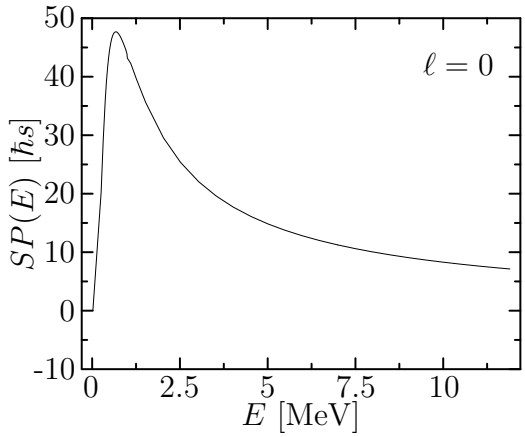

Figure 1.14: $\ell = 0$ speed plot for an α-α system in the grid representation. The peak does not correspond to any resonance.

the resonance is several orders of magnitude smaller than its energy. It is to be observed that the bigger the ratio Γ/E is, the higher the order of the polynomial needed for the background. Note that the quoted error bars are only the statistical error of the fit. The uncertainties for the broader resonances due to the choice of the energy range considered for the fit are larger. The choice of the background also significantly influences the results.

The need for a background can be better seen in the speed plots (Fig. 1.13). $\ell = 2$ shows the strongest asymmetry in the peak related to the resonance, whilst it is hard to perceive any asymmetry at all for $\ell = 0$. The speed plot for $\ell = 0$ is depicted in Fig. (1.14) for energies up to 12 MeV. The broad peak is not associated with the presence of a resonance. In fact, the time delay associated with this peak is negative, whereas the time delay of a resonance is always positive.

1.4 Boundary conditions in a general basis

The next step towards the application of boundary conditions in a realistic many-body model, is the use of a basis for the relative motion that consists of localized states which have an extension in space. For example, in the Cluster Model the Hilbert space for the relative motion is spanned by a set of gaussians.

In Fermionic Molecular Dynamics where the width of the single-particle gaussians need not be equal, the relative motion will reside in a gaussian-like wave-packet. Therefore we study as a first schematic model the representation of the relative motion in terms of gaussians.

Eigenvalue problem in a general basis

For practical applications where an analytic solution of the Schrödinger equation is not possible some kind of discretization of the integral in Eq. (1.2) is usually needed to represent $\big|\, \Psi_r(k,\ell,J)\,\big\rangle$. Outside the range of the nuclear potential, a matching of the interior numerical solution to the exterior analytically known asymptotic state has to be performed, as in the grid representation.

We have a given set of nonorthogonal states $\{\big|\, q_i\,\big\rangle;\ i=1,2,\dots\}$ that spans a Hilbert space and a subset $\{\big|\, q_i\,\big\rangle;\ i=1,\dots,n+n_B\}$ that spans a subspace with which we intend to describe the interior solution. However, in contrast to the grid representation, these states $\big|\, q_i\,\big\rangle$ are not very well localized in the relative distance and overlap with each other (for example gaussians, see Fig. (1.16)).

A linear combination of these states is used to represent the solution $\big|\, u(k,\ell,J)\,\big\rangle$:

$$\big|\, u(k,\ell,J)\,\big\rangle = \sum_{i=1}^{\infty} \Psi_i \big|\, q_i\,\big\rangle, \quad \Psi_i \in \mathbb{C}. \tag{1.38}$$

Let us denote the asymptotic solution by $\big|\, w(k,\ell,J)\,\big\rangle$. Like the eigenstate it can be represented in terms of $\big|\, q_i\,\big\rangle$

$$\big|\, w(k,\ell,J)\,\big\rangle = \sum_{i=1}^{\infty} w_i \big|\, q_i\,\big\rangle. \tag{1.39}$$

The matching or boundary condition can be written as

$$w_i = \Psi_i \text{ for } i = n+1, n+2, \dots, \infty. \tag{1.40}$$

The task is to find the set of coefficients $\vec{\Psi} = \{\Psi_i; i = 1,\dots,n+n_B\}$ such that $\big|\, u(k,\ell,J)\,\big\rangle$ is an eigenstate of the Hamiltonian $\underset{\sim}{H}_r$ under these boundary conditions:

$$\begin{aligned} &\underset{\sim}{H}_r \big|\, u(k,\ell,J)\,\big\rangle = E_{\ell J} \big|\, u(k,\ell,J)\,\big\rangle \\ &f^s_{k\ell J}(\Psi_1,\dots,\Psi_{n+n_B}) = 0, \quad s = 1,\dots,n_B, \end{aligned} \tag{1.41}$$

where the functions $f^s_{k\ell J}$ represent the boundary conditions.

Note that, although the set of coefficients $\vec{\Psi}$ depend on the quantum numbers, this dependence is omitted to retain the simplicity of the notation.

Homogeneous linear boundary condition equations

In the most general case, where $\left| q_i \right\rangle$ will be an antisymmetric many-body state of indistinguishable particles, the relative distance between two sub-clusters is not well defined in the interior region. The index i in $\left| q_i \right\rangle$ labels more the overall extension of the system rather than a well defined distance. Asymptotically one has the channel states (1) where the sub-clusters are clearly distinguishable and their relative distance can be defined.

The asymptotic solution for $\left| \Psi_r(k,\ell,J) \right\rangle$ is usually given in terms of a relative coordinate representation:

$$\left\langle r > R \right| \Psi_r(k,\ell,J) \left\rangle = \frac{w_{k\ell J}(r)}{r} \right| (\ell I_{12}) JM \left\rangle \tag{1.42}$$

Hence, one has to find a corresponding representation for the many-body state $\left| \Psi(k,\ell,J) \right\rangle$ in the region where it is matched to $w_{k\ell J}(r)$. For that we use an operator called $\underset{\sim}{B}$ which measures the spatial extent of the system. In chapter 2, where we treat the microscopic many-body problem, this will be defined as $\underset{\sim}{B} = 1/A^2 \sum_{i<j} (\vec{\underset{\sim}{r}}(i) - \vec{\underset{\sim}{r}}(j))^2$. But here, where we concentrate on the implementation of the boundary conditions in terms of the fuzzy states $\left| q_i \right\rangle$, we do not consider the intrinsic state $\left| \Psi^{I_1}_{\mathrm{C1}} \right\rangle \otimes \left| \Psi^{I_2}_{\mathrm{C2}} \right\rangle$ but consider only the relative motion $\left| \Psi_r(k,\ell,J) \right\rangle$.

In this schematic model we can make comparisons to the coordinate representation, but we will express everything in terms of operators and states, which will keep the discussion more general. We will benefit from this formulation in Chapter 2, where an explicit relative coordinate representation will not be available.

The operator corresponding to the derivative in coordinate space is the conjugate variable of $\underset{\sim}{r}$, related to the velocity:

$$\dot{\underset{\sim}{r}} = \frac{i}{\hbar} \big[\underset{\sim}{H}_r, \underset{\sim}{r} \big] \;\Rightarrow\; -\frac{i\hbar}{\mu} \frac{d}{dr}. \tag{1.43}$$

In this simple case, $\dot{\underset{\sim}{r}} = \underset{\sim}{p}/\mu$; that is, the conjugate variable of r is the momentum p. The representation in coordinate space helps to visualize the meaning of this observable. Thus the n-th power of the velocity operator, $\dot{\underset{\sim}{r}}^n$, corresponds to the n-th derivative with respect to r.

The boundary condition stated in Eq. (1.8) in terms of states, reads:

$$\left\langle r \right| u(k,\ell,J) \left\rangle = \left\langle r \right| w(k,\ell,J) \left\rangle, \quad r \geq R. \tag{1.44}$$

In terms of a Taylor expansion at the matching point $r = R$, this condition is equivalent to matching all derivatives at R:

$$\left\langle R \right| \dot{\underset{\sim}{r}}^s \left| u(k,\ell,J) \right\rangle = \left\langle R \right| \dot{\underset{\sim}{r}}^s \left| w(k,\ell,J) \right\rangle, \quad s = 0,1,2,\ldots. \tag{1.45}$$

For practical purposes, only a few of these need to be implemented. For a set of homogeneous and linear equations in the coefficients Ψ_i, Eq. (1.45) for $s = 0,\ldots,n_B$ can be

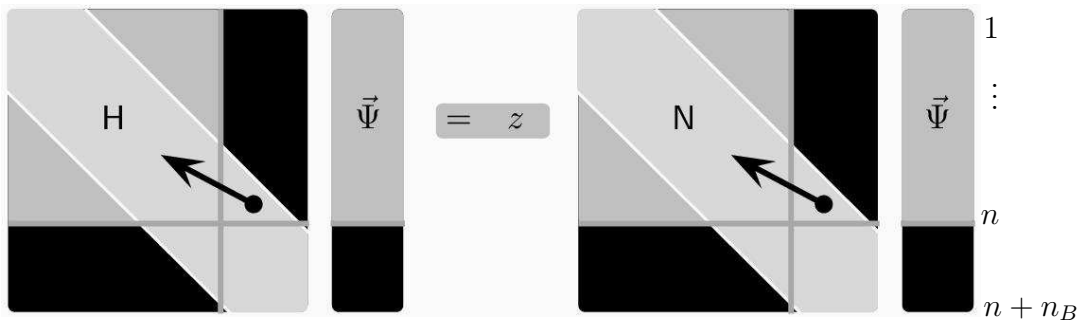

Figure 1.15: Graphical illustration to show the meaning of the imposition of boundary conditions ($z = \frac{\hbar^2}{2\mu}k_{\ell J}^2$).

rewritten as

$$\frac{\left\langle R \left| \underset{\sim}{\dot{r}}^s \right| u(k,\ell,J) \right\rangle}{\left\langle R \left| u(k,\ell,J) \right\rangle} = \frac{\left\langle R \left| \underset{\sim}{\dot{r}}^s \right| w(k,\ell,J) \right\rangle}{\left\langle R \left| w(k,\ell,J) \right\rangle}, \quad s = 1, \ldots, n_B. \tag{1.46}$$

These quotients for the asymptotic solution are in general complex numbers:

$$A_{k\ell J}^s := \frac{\left\langle R \left| \underset{\sim}{\dot{r}}^s \right| w(k,\ell,J) \right\rangle}{\left\langle R \left| w(k,\ell,J) \right\rangle}, \quad s = 1, \ldots, n_B. \tag{1.47}$$

Hence, Eq. (1.46) can be rewritten as

$$\left\langle R \left| \underset{\sim}{\dot{r}}^s - A_{k\ell J}^s \right| u(k,\ell,J) \right\rangle = 0, \quad s = 1, \ldots, n_B. \tag{1.48}$$

or in the form:

$$\sum_{i=1}^{n+n_B} \Psi_i \left\langle R \left| \underset{\sim}{\dot{r}}^s - A_{k\ell J}^s \right| q_i \right\rangle = 0, \quad s = 1, \ldots, n_B, \tag{1.49}$$

where the linearity in the coefficients Ψ_i and the homogeneity of the equations is clearly seen. This allows the implementation of the boundary conditions in the dynamical equation, obtaining an eigenvalue problem with modified matrix elements.

Implementation of the boundary conditions

The eigenvalue problem (3) for the trial state (1.38) can be rewritten

$$\sum_{j=1}^{\infty} \left\langle q_i \left| \underset{\sim}{H}_r \right| q_j \right\rangle \Psi_j = \frac{\hbar^2}{2\mu} k_{\ell J}^2 \sum_{j=1}^{\infty} \left\langle q_i \left| q_j \right\rangle \Psi_j. \tag{1.50}$$

Abbreviating matrix elements and overlaps as

$$\mathsf{H}_{ij} = \left\langle\, q_i \,\middle|\, \underset{\sim}{H}_r \,\middle|\, q_j \,\right\rangle, \quad \mathsf{N}_{ij} = \left\langle\, q_i \,\middle|\, q_j \,\right\rangle, \tag{1.51}$$

equation (1.50) takes the form

$$\sum_{j=1}^{\infty} \mathsf{H}_{ij}\Psi_j = \frac{\hbar^2}{2\mu} k_{\ell J}^2 \sum_{j=1}^{\infty} \mathsf{N}_{ij}\Psi_j. \tag{1.52}$$

The boundary condition equations as expressed in Eq. (1.49) allow us to write the coefficients $\{\Psi_i;\ i > n\}$, as a linear combination of the ones inside the boundary:

$$\Psi_i = \sum_{j=1}^{n} s_{ij}\Psi_j, \quad i = n+1, n+2, \dots\ . \tag{1.53}$$

Note that the coefficients s_{ij} depend on the matching point, energy and quantum numbers. To preserve the simplicity of the notation this is omitted. s_{ij} will fall off with increasing difference in $|i-j|$ because the overlap between two states $\left\langle\, q_i \,\middle|\, q_j \,\right\rangle$ decreases (for an example with gaussians, see Fig. (1.17)). Therefore there will be a certain value $n + n_B$ for which $\Psi_{j>n+n_B} = 0$ and thus all summations over j will effectively run only up to $j = n + n_B$, not up to infinity.

Separating the sums in Eq. (1.52) into two parts,

$$\sum_{j=1}^{n} \mathsf{H}_{ij}\Psi_j + \sum_{l=n+1}^{\infty} \mathsf{H}_{il}\Psi_l = \frac{\hbar^2}{2\mu} k_{\ell J}^2 \left(\sum_{j=1}^{n} \mathsf{N}_{ij}\Psi_j + \sum_{l=n+1}^{\infty} \mathsf{N}_{il}\Psi_l \right) \tag{1.54}$$

and using the boundary condition equations (1.53):

$$\begin{aligned} \sum_{j=1}^{n} \mathsf{H}_{ij}\Psi_j + \sum_{l=n+1}^{n+n_B} \mathsf{H}_{il}\Big(\sum_{j=1}^{n} s_{lj}\Psi_j \Big) &= \frac{\hbar^2}{2\mu} k_{\ell J}^2 \left(\sum_{i=1}^{n} \mathsf{N}_{ij}\Psi_j + \sum_{l=n+1}^{n+n_B} \mathsf{N}_{il}\Big(\sum_{j=1}^{n} s_{lj}\Psi_j \Big) \right) \\ \sum_{j=1}^{n} \Big(\mathsf{H}_{ij} + \sum_{l=n+1}^{n+n_B} \mathsf{H}_{il}\ s_{lj} \Big)\Psi_j &= \frac{\hbar^2}{2\mu} k_{\ell J}^2 \sum_{j=1}^{n} \Big(\mathsf{N}_{ij} + \sum_{l=n+1}^{n+n_B} \mathsf{N}_{il}\ s_{lj} \Big)\Psi_j, \end{aligned} \tag{1.55}$$

we again get an eigenvalue problem, but the matrix elements are modified by the boundary conditions. The modification consists of adding the off diagonal matrix elements H_{il} and N_{il}, weighted by the influence s_{lj} of the amplitude Ψ_j on the amplitude Ψ_l according to the boundary conditions. A graphical explanation of this is given in Fig. (1.15). The squares represent Hamiltonian and overlap matrices and the columns represent the amplitudes $\vec{\Psi}$. Two diagonal lines define a band in which the matrix elements are not negligible. The dark squares represent the matrices up to n, the whole square represents the matrices up to $n+n_B$. As can be seen, a simple cut at n leaves out the coupling to the n_B components

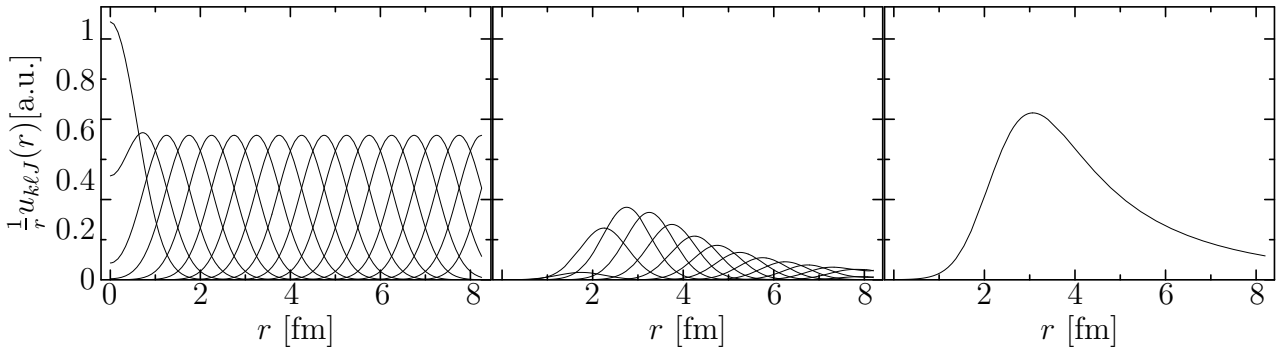

Figure 1.16: The α-α system for $\ell = 0$ in a gaussian representation. From left to right: basis, contribution $\frac{1}{r}\left(\left\langle\, r \,\middle|\, g_i \,\right\rangle + \left\langle\, r \,\middle|\, g_{-i} \,\right\rangle\right)$ for each $i = 1, \ldots, n$ and wave function $\frac{1}{r}\left\langle\, r \,\middle|\, u(k,0,0) \,\right\rangle$. Note the influence of the contributions from $i = n+1, \ldots, n+n_B$ seen close to the boundary at $R = d_n = 8.25$ fm that originate in the boundary conditions.

outside, due to the matrix elements in the triangles. This is included in the smaller matrices by means of the boundary conditions, represented by the arrow.

Figure (1.16) illustrates the implementation of boundary conditions for a gaussian basis (see the following section for details). The wave function is described up to the matching point by Eq. (1.38) with the boundary conditions (1.53), resulting in

$$\left\langle\, r \,\middle|\, u(k,\ell,J) \,\right\rangle = \sum_{i=1}^{n} \Psi_i \Big(\left\langle\, r \,\middle|\, q_i \,\right\rangle + \sum_{i=n+1}^{n+n_B} s_{ij} \left\langle\, r \,\middle|\, q_j \,\right\rangle \Big). \tag{1.56}$$

Thus, the contribution of each term is modified by the gaussians outside according to the boundary conditions coded in s_{ij}.

1.5 Set of gaussians spanning a Hilbert space

The coordinate part of an FMD state is represented by a gaussian. Thus, it is natural to take as the next step the use of a gaussian basis to solve the same problems as in Sec. 1.3.

1.5.1 Formulation of the problem

We consider the following trial state:

$$\big|\, u(k,\ell,J)\,\big\rangle = \sum_{i=1}^{n+n_B} \Psi_i \,\Big(\, \big|\, g_i\,\big\rangle + \big|\, g_{-i}\,\big\rangle \,\Big) \tag{1.57}$$

where the basis is a set of displaced gaussians for the radial wave function

$$\big\langle\, r \,\big|\, g_i\,\big\rangle = g_i(r) = r e^{-\frac{(r-d_i)^2}{2a}}. \tag{1.58}$$

The centers of the gaussians are regularly distributed at different relative distances, avoiding d_0:

$$\left.\begin{aligned} d_i &= (i-\frac{1}{2})\ \Delta_g, \\ d_{-i} &= (-i+\frac{1}{2})\ \Delta_g, \end{aligned}\right\} \qquad i = 1,2,3,\ldots \tag{1.59}$$

This choice of trial state naturally includes the boundary condition at $r=0$ for the $\ell=0$ radial problem (see Sec.(1.3.1)). In addition, it helps to calculate the matrix elements. By mathematically defining the continuation of the r variable on the negative axis and $V_\ell(r) = V_\ell(-r)$, the integrals can be transformed into:

$$\begin{aligned} \big\langle\, u(k,\ell,J)\,\big|\,\underset{\sim}{V}_\ell\,\big|\,u(k,\ell,J)\,\big\rangle &= \int_0^\infty dr\ \ \big\langle\, u(k,\ell,J)\,\big|\,r\,\big\rangle V_\ell(r) \big\langle\, r\,\big|\,u(k,\ell,J)\,\big\rangle \\ &= \int_0^\infty dr\ \ \sum_{i,j=1}^{\infty} \Psi_i^*\Psi_j \Big(g_i(r)+g_{-i}(r)\Big) V_\ell(r) \Big(g_j(r)+g_{-j}(r)\Big) \\ &= \sum_{i,j=1}^{\infty} 2\Psi_i^*\Psi_j \Big(\big\langle\, g_i\,\big|\,\underset{\sim}{V}_\ell\,\big|\,g_j\,\big\rangle + \big\langle\, g_i\,\big|\,\underset{\sim}{V}_\ell\,\big|\,g_{-j}\,\big\rangle\Big), \end{aligned} \tag{1.60}$$

where we define:

$$\begin{aligned} \big\langle\, g_j\,\big|\,\underset{\sim}{V}_\ell\,\big|\,g_i\,\big\rangle &= \int_{-\infty}^{\infty} dr\ \ g_i(r) V_\ell(r) g_j(r) \\ \big\langle\, g_j\,\big|\,g_i\,\big\rangle &= \int_{-\infty}^{\infty} dr\ \ g_i(r) g_j(r). \end{aligned} \tag{1.61}$$

It should be noted that the kinetic energy matrix elements $\langle\, g_j \,|\, \underset{\sim}{T} \,|\, g_i \,\rangle$ and overlaps $\langle\, g_j \,|\, g_i \,\rangle$ can be calculated analytically, and that the dimension of the matrices is between one and two orders of magnitude lower than in the case of a grid, for the same accuracy.

With this trial state and the former manipulation to calculate the matrix elements, the eigenvalue problem is

$$\sum_{i=1}^{\infty} \big(\langle\, g_j \,|\, \underset{\sim}{H}_r \,|\, g_i \,\rangle + \langle\, g_j \,|\, \underset{\sim}{H}_r \,|\, g_{-i} \,\rangle\big)\Psi_i = E \sum_{i=1}^{\infty} \big(\langle\, g_j \,|\, g_i \,\rangle + \langle\, g_j \,|\, g_{-i} \,\rangle\big)\Psi_i. \tag{1.62}$$

The choice of the basis determines the number n_B of boundary condition equations that are needed. Choosing $R = d_n$, all gaussians that have a significant contribution to the wave function $\langle\, R \,|\, \Psi_r(k,\ell,J) \,\rangle$ must be included in the formulation of the problem to give a complete description of the system for $r \leq R$. In terms of matrix elements n_B has to be chosen such that:

$$\begin{aligned} \langle\, g_n \,|\, \underset{\sim}{H}_r \,|\, g_{n+n_B} \,\rangle &\ll \langle\, g_n \,|\, \underset{\sim}{H}_r \,|\, g_n \,\rangle, \\ \langle\, g_n \,|\, g_{n+n_B} \,\rangle &\ll \langle\, g_n \,|\, g_n \,\rangle. \end{aligned} \tag{1.63}$$

Thus, adding more states $|\, q_{n+n_b+i} \,\rangle$ will not affect the description of the system for $r \leq R = d_n$.

1.5.2 Results

Equation (1.62) under the conditions (1.49) can be solved as explained in the previous section. The particular cases under consideration are again the systems n-α and α-α, with

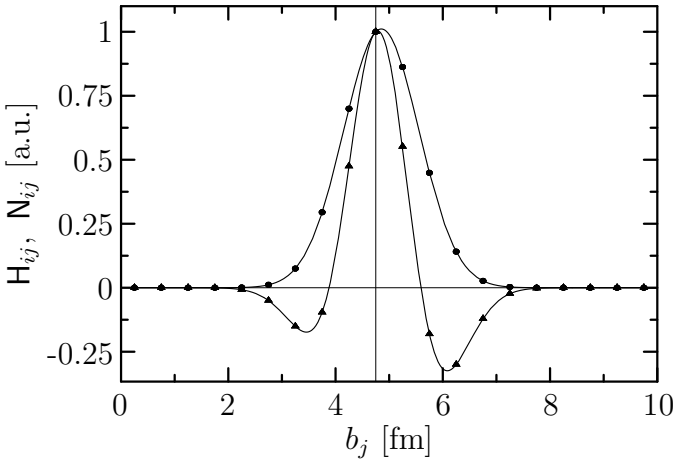

Figure 1.17: Normalized overlap (dots) and Hamiltonian matrix elements (triangles) for a basis of gaussians, $i = 10,\ d_i = 4.75$ fm.

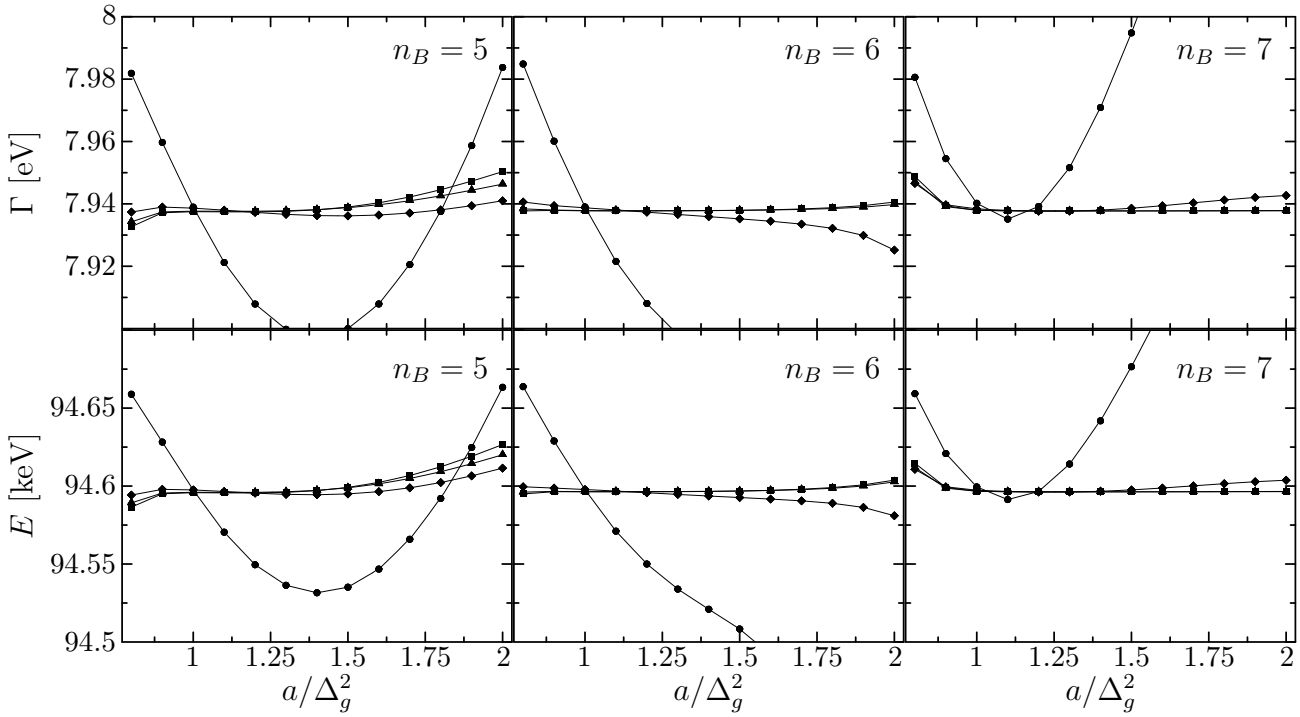

Figure 1.18: Energy E and width Γ for the α-α $\ell = 0$ case, shown in a gaussian representation. The result is optimized by choosing the value of a/Δ_g. Curves for $1/\Delta_g = 2, 2.5, 3, 3.5$ fm^{-1} are represented by circles, diamonds, triangles and squares, respectively. For $n_B = 6$ and 7, the triangles and squares are indistinguishable. Results obtained in the grid representation: $E = 94.6$ keV,$\Gamma = 7.93$ eV.

the same interactions as used in Sec.1.3. The results in that section are taken as a reference. For the application to the n-α system, the matrix elements of the interaction need to be calculated by numerical integrals, but the potential in the α-α system can be integrated analytically within the chosen basis. We therefore start by discussing the α-α case.

	$\ell = 0$		$\ell = 2$		$\ell = 4$	
	E [MeV]	Γ [eV]	E [MeV]	Γ [MeV]	E [MeV]	Γ [MeV]
Gamov Vector	0.0946	7.94	2.90	1.28	11.6	3.11

Table 1.3: Resonance parameters for the α-α system calculated using a gaussian basis.

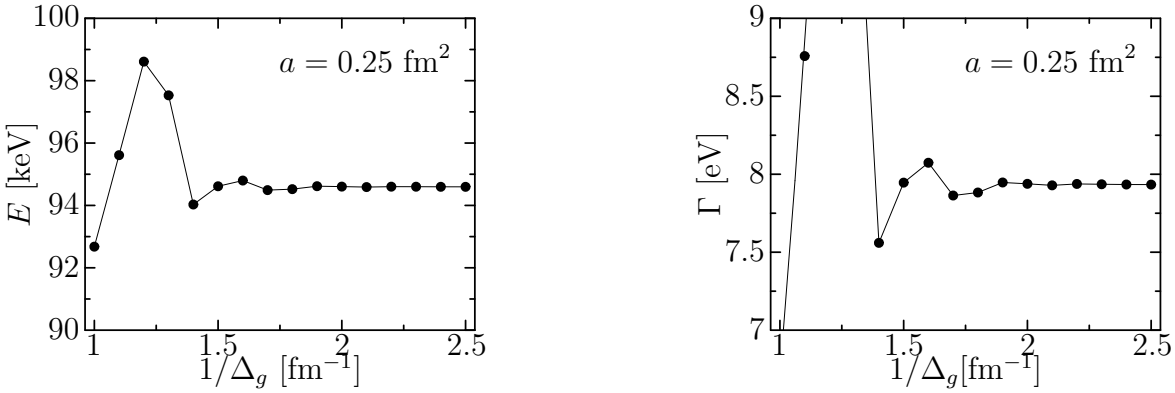

Figure 1.19: Convergence of E and Γ for the α-α $\ell = 0$ system in a gaussian representation as a function of $1/\Delta_g$.

Coulomb wave

The maximum value of the width of the gaussian is related to the shape of the potential well. If the gaussians cannot represent the radial wave function the basis is not adequate. Hence, the higher the energy of the state, the higher the degree of bending in the wave function and the narrower the gaussians must be. This will be of crucial importance in the next chapter, since the microscopic description of nuclei will impose a certain width for the relative motion and in consequence an upper limit to the energy range in which we can describe the states. Moreover, the width a and the separation Δ_g are correlated: if neighbouring gaussians have little overlap, the basis will not cover the Hilbert space and if they have too much, the basis will be overcomplete, leading to numerical problems due to zero eigenvalues of the overlap matrix. The optimum combination of a and Δ_g yielded by

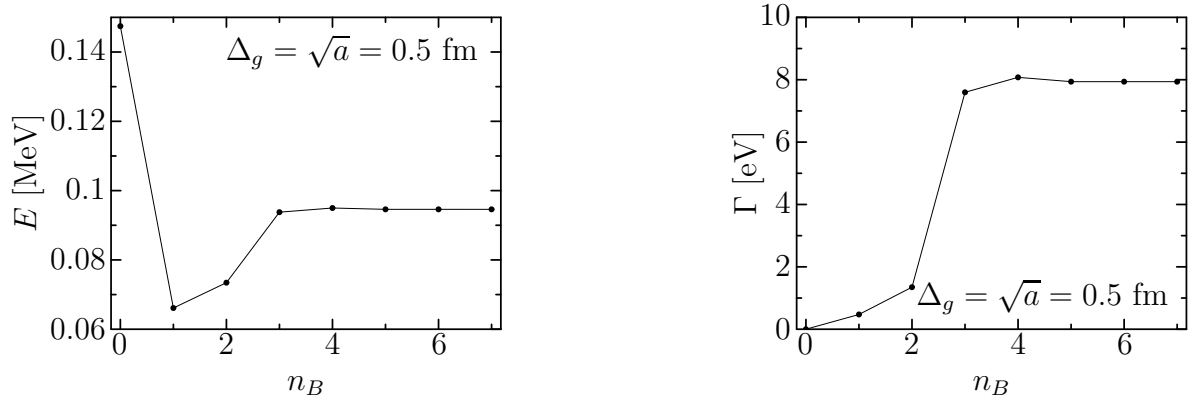

Figure 1.20: Convergence of the resonance energy and width plotted against the number of boundary condition equations n_B, for the α-α $\ell = 0$ case in a gaussian representation.

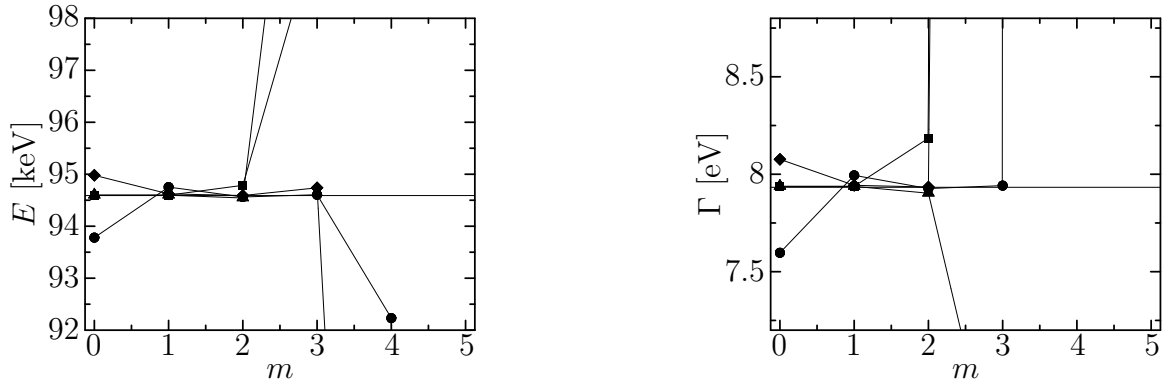

Figure 1.21: Convergence of the energy and width of the resonance applying boundary conditions at $R = d_{n-m}$ for the α-α $\ell = 0$ system in a gaussian representation. Lines are drawn for $n_B = 3, 4, 5$ and 6 (circle, diamond, triangle and square, respectively).

the tests is $a \lesssim 0.25$ fm^2 and $\Delta_g \leq \sqrt{a}$ (see Fig. (1.18)). For $a = 1.1\Delta_g^2$, the convergence in Δ_g is perfect for $\Delta_g \leq 0.4$ fm. Note also the convergence with $1/\Delta_g$ shown in Fig. (1.19).

The number of boundary condition equations required can be estimated by evaluating the matrix elements and overlaps. Figure (1.17) shows these quantities for the α-α $\ell = 0$ case, with $\Delta_g = 0.5$ fm and $a = 0.25$ fm^2. Less than $n_B = 5$ equations would not yield a complete description of the system for the chosen relation between gaussian separation and width. However, the sixth equation would not contain any additional information. This is confirmed by the calculation, as shown in Fig. (1.20). Note that the amount of boundary condition equations n_B depends on the degree of overlap between neighbouring gaussians: a larger overlap requires more equations (see Fig. (1.18)).

A possibility to reduce the number of boundary condition equations is to apply them

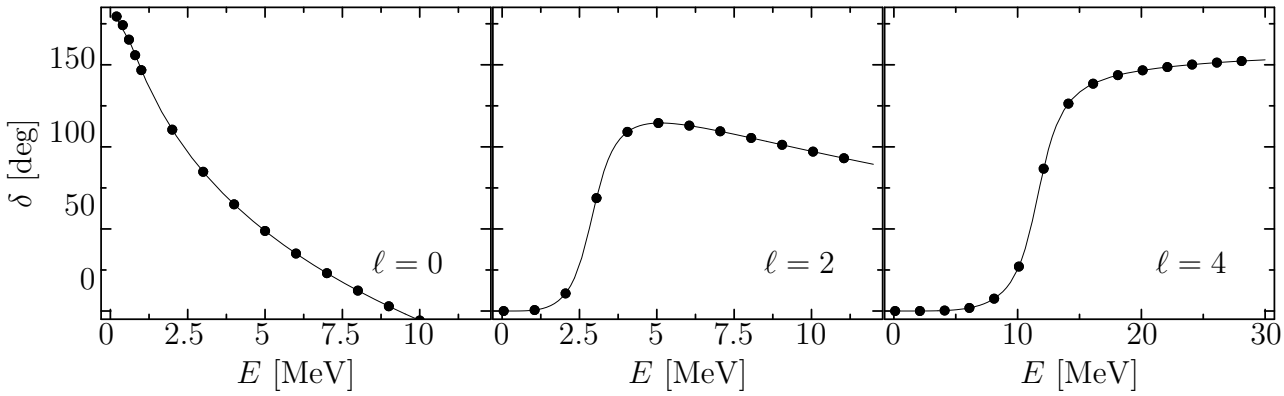

Figure 1.22: The circles depict phase shifts for the α-α system calculated in a gaussian basis and the solid lines represent the reference calculated in the grid representation.

	$p_{3/2}$		$p_{1/2}$	
	E [MeV]	Γ [eV]	E [MeV]	Γ [MeV]
Gamov Vector	0.840	0.552	2.91	4.60

Table 1.4: Resonance parameters for the n-α system calculated with a gaussian basis.

at $R = d_{n-m}$. Then, conditions (1.63) will be fulfilled for a smaller n_B, as shown in Fig. (1.21). Nevertheless, numerical problems arise since the involved overlaps become very small and produce a set of numerically unstable equations.

According to these findings, all calculations are performed for the following parameterization:

$$\Delta_g = 0.5 \text{ fm}, \quad a = 1.1\Delta_g^2, \quad n_B = 5. \tag{1.64}$$

The matching point R depends on the potential under consideration and in general is chosen such that the relative difference between total potential and Coulomb plus centrifugal barrier, is less than 0.05%. Nevertheless, even if this condition is fulfilled, the amount of n free parameters in $\vec{\Psi}$ must be large enough to describe the wave function in the region of interest, thus setting a minimum value for R.

Final results for the resonances in the α-α system are displayed in Table (1.3) and should be compared to those in Table (1.2). The agreement with the reference figures is excellent. Moreover, the solution given by the grid method converges to the one obtained by the gaussian basis as the grid size is decreased, whilst the latter remains unchanged by variations in the parameters n_B, Δ_g and a; providing these variations are kept within the margins required for a good description of the Hilbert space.

Phase shifts can also be calculated in this basis. The results match with the previous ones, up to the numerical precision of the calculation. A comparison between them is presented in Fig. (1.22).

Free spherical wave

The accuracy of the calculation is the n-α case limited by the use of numerical integration. The discrepancy between the results and the reference figures is nevertheless low, being in all cases less than 1.3% (compare Table (1.4) with Table (1.1)). Similar agreement is obtained for the phase shifts and the Pauli forbidden bound state.

1.6 Relative distance representation

In this section we investigate within the framework of our schematic model, the properties of a distance operator that is in accordance with quantum mechanics for indistinguishable particles. When the clusters overlap strongly, the ansatz (1) that factorizes the nuclear system into relative motion between the fragments and intrinsic states and hence is well suited for the asymptotic region, can no longer be maintained or even makes much sense. For example this is the case in microscopic models, in which the many-body state is described in terms of single-particle states and the relative and center of mass motion cannot be factorized out. The situation is even more intricate when antisymmetrization is considered, as it should be. For example in the case of ^{5}He there is no way to define the distance between the last neutron and the ^{4}He nucleus. The classical expression would be

$$\vec{x}_{n-\alpha} = \vec{x}(5) - \frac{1}{4}\sum_{i=1}^{4}\vec{x}(i) \tag{1.65}$$

where $\vec{x}(1),\ldots,\vec{x}(4)$ denote the positions of nucleons belonging to the ^{4}He nucleus and $\vec{x}(5)$ denotes the position of the last neutron.

If we regard $\vec{x}_{n-\alpha}$ as an operator in the antisymmetric subspace we find that it vanishes:

$$\begin{aligned}\underset{\sim}{\mathcal{A}}\;\underset{\sim}{\vec{x}}_{n-\alpha}\;\underset{\sim}{\mathcal{A}} &= \underset{\sim}{\mathcal{A}}\;\sum_{\mathcal{P}}\Big(\underset{\sim}{\vec{x}}(\mathcal{P}(5)) - \frac{1}{4}\sum_{i=1}^{4}\underset{\sim}{\vec{x}}(\mathcal{P}(i))\Big)\;\underset{\sim}{\mathcal{A}}\\ &= \underset{\sim}{\mathcal{A}}\;\Big(\sum_{j=1}^{5}\underset{\sim}{\vec{x}}(j) - \frac{1}{4}\sum_{i=1}^{4}\sum_{j=1}^{5}\underset{\sim}{\vec{x}}(j)\Big)\;\underset{\sim}{\mathcal{A}} = 0,\end{aligned} \tag{1.66}$$

where $\mathcal{P}$ denotes all possible particle permutations and $\underset{\sim}{\mathcal{A}}$ denotes the antisymmetrization operator. This simple example shows that for indistinguishable particles, we need to find a quantum mechanically correct operator that plays the role of the relative distance.

In the asymptotic region this distance measure has to have a one-to-one correspondence with the classical distance, in order to incorporate the boundary conditions that are expressed in terms of the channel states (1).

When the clusters are well separated one can define operators $\underset{\sim}{\theta}_{\text{left}}$ and $\underset{\sim}{\theta}_{\text{right}}$, that project on the space left and right of a dividing surface and one can define

$$\underset{\sim}{\vec{x}}_{n-\alpha} = \frac{1}{\left\langle\,\underset{\sim}{\theta}_{\text{left}}\,\right\rangle}\sum_{i=1}^{5}\underset{\sim}{\vec{x}}(i)\;\underset{\sim}{\theta}_{\text{left}} - \frac{1}{\left\langle\,\underset{\sim}{\theta}_{\text{right}}\,\right\rangle}\sum_{i=1}^{5}\underset{\sim}{\vec{x}}(i)\;\underset{\sim}{\theta}_{\text{right}}. \tag{1.67}$$

This is a quantum mechanically correct operator and reduces to the classical expression (1.65) if the neutron is entirely left and the ^{4}He nucleus is entirely right of the dividing surface. But we see already that this definition will not work if the relative motion is in an eigenstate of angular momentum. Since an $\ell = 0$ state is rotationally invariant and a dividing surface does not exist, one would get $\left\langle\,\underset{\sim}{\theta}_{\text{left}}\,\right\rangle = \left\langle\,\underset{\sim}{\theta}_{\text{right}}\,\right\rangle = 5/2$ and $\underset{\sim}{\vec{x}}_{n-\alpha} = 0$.

1.6.1 Formal definition of a relative distance

All observables that permit a one-to-one mapping with the relative distance between the fragments in the asymptotic region, are candidates to define a relative distance measure $\underset{\sim}{B}$. One would think, for example, of the size of the system, the quadrupole deformation, or even the Coulomb energy between the fragments. All these physical quantities, as well as many others, can be related to the relative distance between the centers of mass of both fragments in the asymptotic region, which is where the boundary conditions are to be imposed. However, for many-body states with good angular momentum the distance measure $\underset{\sim}{B}$ should be rotationally invariant, so the quadrupole moment is excluded.

Without explicitly specifying the distance measure $\underset{\sim}{B}$ in terms of the single-particle variables, let us first discuss the general concept. The spectral representation of the observable $\underset{\sim}{B}$ is

$$\underset{\sim}{B} = \sum_{i=1}^{\infty} \left| b_i \right\rangle \, b_i \, \left\langle b_i \right|. \tag{1.68}$$

In general the spectrum may be continuous, but for practical applications one is usually restricted to a discrete representation. If the observable $\underset{\sim}{B}$ is suitably chosen, the eigenvalues b_i can be related in a unique way to a relative distance r in the asymptotic region, by

$$r_i = r(b_i), \tag{1.69}$$

$r(b)$ can be continued into the region where the clusters overlap, provided that the mapping is bijective, in other words $r(b)$ should be monotonic. As an example one may think of the average inter-particle distance

$$\underset{\sim}{B} = \frac{1}{A^2} \sum_{i<j=1}^{A} \left(\underset{\sim}{\vec{x}}(i) - \underset{\sim}{\vec{x}}(j) \right)^2. \tag{1.70}$$

In this case, which will also be used in Chapter 2,

$$r(b) = \sqrt{\left(A\, b - A_1\, r_{\mathrm{C1}}^2 - A_2\, r_{\mathrm{C2}}^2 \right) / \mu_A}, \tag{1.71}$$

where r_{C1} and r_{C2} are the rms-radii of the two asymptotic clusters, $\mu_A = \mu/m$ is the mass number of the system and m is the nucleon mass (see Sec. 2.2.2 for details). The eigenstates $\left| b_i \right\rangle$ can then be used to define the relative distance operator:

$$\underset{\sim}{R} = \sum_{i=1}^{\infty} \left| b_i \right\rangle \, r(b_i) \, \left\langle b_i \right|. \tag{1.72}$$

In practice, the eigenstates of $\underset{\sim}{B}$ will be obtained by solving the eigenvalue problem in a finite dimensional Hilbert space, thus $\underset{\sim}{B}$ will be approximated by

$$\underset{\sim}{B} \approx \sum_{i=1}^{N} \left| b_i \right\rangle \, b_i \, \left\langle b_i \right| \quad \text{and} \quad \underset{\sim}{B}^2 \approx \sum_{i=1}^{N} \left| b_i \right\rangle \, b_i^2 \, \left\langle b_i \right|. \tag{1.73}$$

As discussed in Sec. 1.6.2, $\underset{\sim}{B}^2$ projected on the subspace is not exactly the same as the square of the projected $\underset{\sim}{B}$. But nevertheless one expects $\left| b_i \right\rangle$ to represent states well localized in the distance measure because in the full Hilbert space the exact eigenstate has no variance: $\left\langle b_i \right| \underset{\sim}{B}^2 \left| b_i \right\rangle = \left\langle b_i \right| \underset{\sim}{B} \left| b_i \right\rangle^2$.

1.6.2 Operators in a restricted Hilbert space

Given a set of non-orthonormalized states:

$$\left\{ \left| q_i \right\rangle, i = 1, \ldots, N \right\} \tag{1.74}$$

spanning a subspace of a Hilbert space (model space), the projection operator $\underset{\sim}{I}$, which is the identity operator in this restricted Hilbert space, is given by

$$\underset{\sim}{I} = \sum_{i,j=1}^{N} \left| q_i \right\rangle \mathsf{O}_{ij} \left\langle q_j \right|. \tag{1.75}$$

An operator $\underset{\sim}{A}$ with matrix elements

$$\mathsf{A}_{ij} = \left\langle q_i \right| \underset{\sim}{A} \left| q_j \right\rangle; \quad i, j = 1, \ldots, N, \tag{1.76}$$

is represented in the restricted Hilbert space as

$$\underset{\sim}{I}\underset{\sim}{A}\underset{\sim}{I} = \left| \vec{q} \right\rangle \cdot \mathsf{O} \cdot \mathsf{A} \cdot \mathsf{O} \cdot \left\langle \vec{q} \right|, \tag{1.77}$$

where

$$\begin{aligned} &\left| \vec{q} \right\rangle = (\left| q_1 \right\rangle, \ldots, \left| q_N \right\rangle), \quad \left\langle \vec{q} \right| = (\left\langle q_1 \right|, \ldots, \left\langle q_N \right|)^T, \\ &\mathsf{O} = \mathsf{N}^{-1}, \quad \mathsf{N} = \{\mathsf{N}_{ij}\}, \quad \mathsf{N}_{ij} = \left\langle q_i \right| \left. q_j \right\rangle, \qquad i, j = 1, \ldots, N \\ &\mathsf{A} = \{\mathsf{A}_{ij}\} \end{aligned} \tag{1.78}$$

and the dot denotes the matrix product. The product of two observables each restricted to this subspace is

$$\begin{aligned} \underset{\sim}{I}\underset{\sim}{C}\underset{\sim}{I} = \underset{\sim}{I}\underset{\sim}{A}\underset{\sim}{I}\underset{\sim}{B}\underset{\sim}{I} &= \left| \vec{q} \right\rangle \cdot \mathsf{O} \cdot \mathsf{A} \cdot \mathsf{O} \cdot \mathsf{N} \cdot \mathsf{O} \cdot \mathsf{B} \cdot \mathsf{O} \cdot \left\langle \vec{q} \right| = \\ &= \left| \vec{q} \right\rangle \cdot \mathsf{O} \cdot \mathsf{A} \cdot \mathsf{O} \cdot \mathsf{B} \cdot \mathsf{O} \cdot \left\langle \vec{q} \right| = \left| \vec{q} \right\rangle \cdot \mathsf{O} \cdot \mathsf{C} \cdot \mathsf{O} \cdot \left\langle \vec{q} \right| \end{aligned} \tag{1.79}$$

where we defined

$$\mathsf{C} = \mathsf{A} \cdot \mathsf{O} \cdot \mathsf{B}. \tag{1.80}$$

One must, however, keep in mind that in general

$$\underset{\sim}{I}\underset{\sim}{A}\underset{\sim}{B}\underset{\sim}{I} \neq \underset{\sim}{I}\underset{\sim}{A}\underset{\sim}{I}\underset{\sim}{B}\underset{\sim}{I}. \tag{1.81}$$

With these expressions it is possible to work with matrices and vectors, instead of, but equivalently to, operators and kets; this makes any calculation easier to handle.

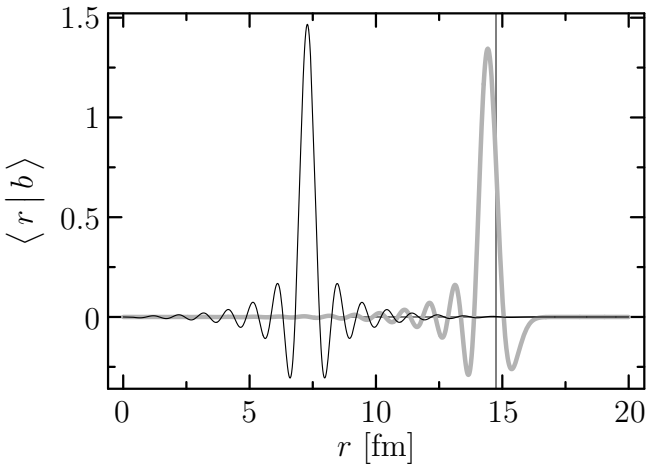

Figure 1.23: Eigenstates of the position operator. The solid black line depicts an eigenstate away from the boundary and the thick grey line, one near the boundary ($R = 14.75$ fm).

1.6.3 Discrete form of the representation

Working in a restricted Hilbert space, only a discrete relative distance representation is possible. According to the ideas expressed in Sec. 1.6.2, the localized states can be expressed in terms of the basis $\big|\, q_i \,\big\rangle$ as

$$\big|\, b_j \,\big\rangle = \sum_{i=1}^{N} \beta_j^{(i)} \big|\, q_i \,\big\rangle, \quad j = 1, \ldots, N. \tag{1.82}$$

The coefficients $\beta_j^{(i)}$are given by the diagonalization of $\underset{\sim}{B}$:

$$\underset{\sim}{B}\big|\, b_j \,\big\rangle = b_j \big|\, b_j \,\big\rangle \quad \Rightarrow \sum_{i=1}^{N} \big\langle\, q_j \,\big|\, \underset{\sim}{B} \,\big|\, q_i \,\big\rangle\, \beta_j^{(i)} = b_j \sum_{i=1}^{N} \big\langle\, q_j \,\big|\, q_i \,\big\rangle\, \beta_j^{(i)}. \tag{1.83}$$

In matrix form:

$$\mathsf{B}\ \vec{\beta}_j = b_j\ \mathsf{N}\ \vec{\beta}_j, \tag{1.84}$$

where

$$\vec{\beta}_j = (\beta_j^{(1)}, \ldots, \beta_j^{(N)}). \tag{1.85}$$

Note that, given the basis (1.74), only N linearly independent states can be constructed.

Eigenstates of $\underset{\sim}{B} = \sqrt{\underset{\sim}{\vec{r}^{\,2}}}$ are shown in Fig. (1.23). The basis $\big|\, q_i \,\big\rangle$ covers positions of the gaussians up to 14.75 fm. The choice of the basis is the same as in Sec. 1.5. The state centered at 7.25 fm is well localized with a narrow width and oscillations symmetric around the mean (shown in black in Fig. (1.23)), whilst the one that peaks near the boundary (shown in grey) is not well represented. The states near the boundaries of the restricted

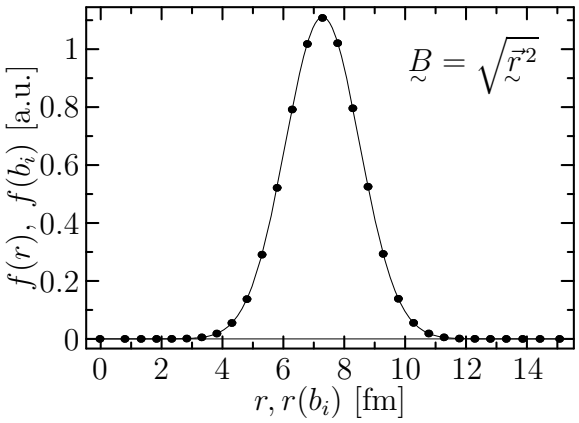

Figure 1.24: Discrete representation of a trial function marked by circles and comparison with the exact one shown by the solid line.

Hilbert space are not so well defined because they are missing the contribution of states outside the boundaries.

Once the states $\{\,|\,b_j\,\rangle, j = 1, \ldots, N\}$ are found, it is possible to define the radial wave function at discrete values of the relative distance, as:

$$u_{k\ell J}(r(b_j)) = r(b_j)\langle\, b_j \,|\, \Psi_r(k, \ell, J)\,\rangle. \tag{1.86}$$

Thus, we have obtained the representation of $|\,u(k, \ell, J)\,\rangle$ in the discrete relative distance variable inside the restricted Hilbert space. In Fig. (1.24) we represent a state

$$|\,f\,\rangle = \sum_{j=1}^{N} f_j\ |\,q_j\,\rangle = \sum_{i=1}^{N} |\,b_i\,\rangle \sum_{j=1}^{N} f_j \langle\, b_i \,|\, q_j\,\rangle = \sum_{i=1}^{N} f(b_i) |\,b_i\,\rangle \tag{1.87}$$

in terms of $f(r) = \langle\, r \,|\, f\,\rangle$ (solid line) and $f(b_i)$ (circles), where $\underset{\sim}{B} = \sqrt{\underset{\sim}{\vec{r}^2}}$. One sees that $f(b_i)$ and $\langle\, r = b_i \,|\, f\,\rangle$ are practically identical. Therefore $|\,b_i\,\rangle$ serves as a relative distance representation.

1.6.4 Implementation of derivatives

For a complete description of the system in the relative distance representation, derivatives with respect to the relative distance are also required. In particular, the boundary condition equations require the use of derivatives.

For a Hamiltonian $\underset{\sim}{H}_r = \underset{\sim}{p}^2/(2\mu) + V(\underset{\sim}{r})$ with a local potential, the time derivative of r is related to the derivative by

$$\dot{\underset{\sim}{r}} = \frac{i}{\hbar}[\underset{\sim}{H}_r, \underset{\sim}{r}] = \frac{\underset{\sim}{p}}{\mu} \quad \Longrightarrow \quad \frac{-i\hbar}{\mu}\frac{d}{dr}, \tag{1.88}$$

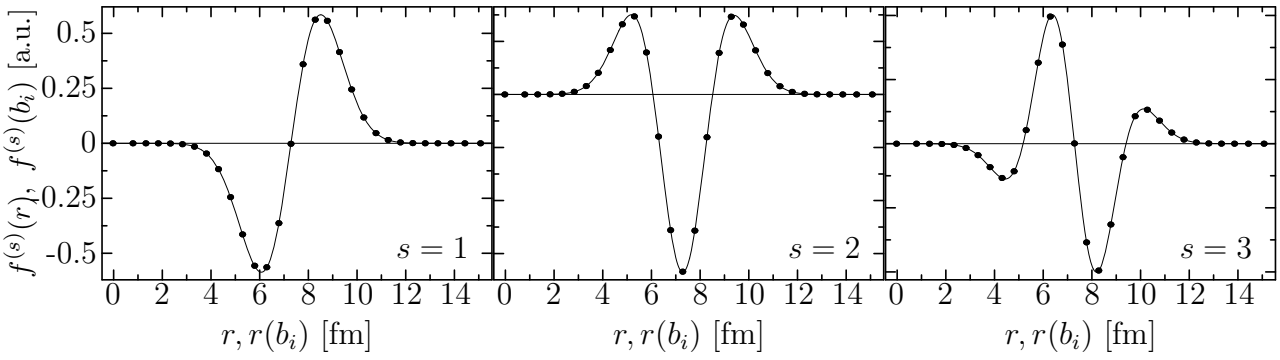

Figure 1.25: Discrete representation of several derivatives of a trial function marked by circles and a comparison with the exact derivatives marked by solid lines. The distance measure operator is the same as in Fig. (1.24).

where μ is the reduced mass of the system and $\underset{\sim}{p}$ is the relative momentum.

The time derivative of $\underset{\sim}{B}$ will also be related to the derivative in the relative coordinate:

$$\dot{\underset{\sim}{B}} = \frac{i}{\hbar}\big[\underset{\sim}{H}, \underset{\sim}{B}\big], \tag{1.89}$$

if $\underset{\sim}{B} = \underset{\sim}{r}$ this fact is obvious (Eq. 1.88). Another example is $\underset{\sim}{B} = \underset{\sim}{r}^2$:

$$\dot{\underset{\sim}{B}} = \dot{\underset{\sim}{r}^2} = \frac{i}{\hbar}\big[\underset{\sim}{H}, \underset{\sim}{r}^2\big] = \frac{1}{\mu}(\underset{\sim}{p}\,\underset{\sim}{r} + \underset{\sim}{r}\,\underset{\sim}{p}) \quad \Longrightarrow \quad \frac{-i\hbar}{\mu}(1 + 2r\frac{d}{dr}). \tag{1.90}$$

Taking powers of $\dot{\underset{\sim}{B}}$ will yield higher derivatives with respect to r.

According to this, for any given trial state $\big|\, u(k,\ell,J)\,\big\rangle$, the derivative is expressed as

$$\frac{du_{k\ell J}(r)}{dr} = -\frac{\mu}{i\hbar}\big\langle\, r \,\big|\, \dot{\underset{\sim}{r}} \,\big|\, u(k,\ell,J)\,\big\rangle, \tag{1.91}$$

but the same information is contained in

$$\big\langle\, b \,\big|\, \dot{\underset{\sim}{B}} \,\big|\, u(k,\ell,J)\,\big\rangle, \tag{1.92}$$

hence it is equivalent to use powers of $\dot{\underset{\sim}{r}}$ or of $\dot{\underset{\sim}{B}}$ for higher derivatives.

In the case of a reduced Hilbert space, the matrix element (1.92) can only be evaluated at discrete points given by the eigenvalues b_j:

$$\frac{du_{k\ell J}(r)}{dr}|_{r=r(b_j)} = f\Big(\big\langle\, b_j \,\big|\, \dot{\underset{\sim}{B}} \,\big|\, u(k,\ell,J)\,\big\rangle,\ \ \big\langle\, b_j \,\big|\, u(k,\ell,J)\,\big\rangle\ , b_j\Big), \tag{1.93}$$

and the same for higher derivatives. For $\underset{\sim}{B} = \underset{\sim}{r}^2$ we obtain

$$\frac{du_{k\ell J}(r)}{dr}|_{r=r(b_j)} = -\frac{1}{2r(b_j)}\left(\big\langle\, b_j \,\big|\, u(k,\ell,J)\,\big\rangle + \frac{\mu}{i\hbar}\big\langle\, b_j \,\big|\, \dot{\underset{\sim}{B}} \,\big|\, u(k,\ell,J)\,\big\rangle\right) \tag{1.94}$$

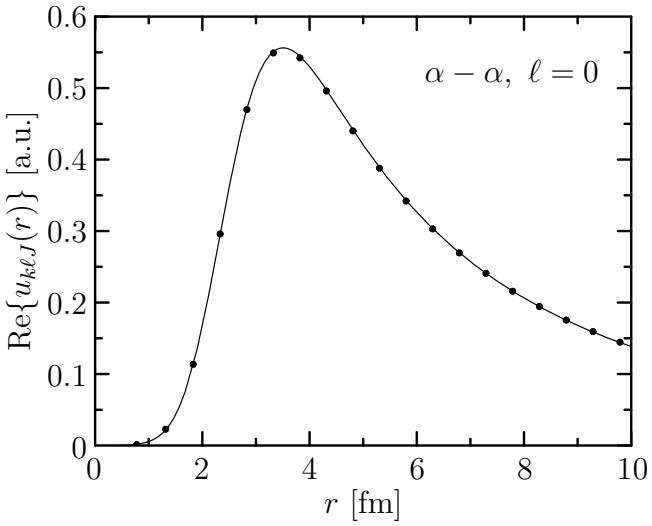

Figure 1.26: The circles show the discrete representation of the wave function for a resonance and the solid line depicts the reference solution.

Figure (1.25) illustrates up to the third derivative for $\underset{\sim}{B} = \underset{\sim}{r}$.

The boundary condition equations (1.46) can be written

$$\frac{\left\langle R \left| (\dot{\underset{\sim}{B}})^s \right| u(k,\ell,J) \right\rangle}{\left\langle R \left| u(k,\ell,J) \right\rangle} = \frac{\left\langle R \left| (\dot{\underset{\sim}{B}})^s \right| w(k,\ell,J) \right\rangle}{\left\langle R \left| w(k,\ell,J) \right\rangle}, \quad s = 1, \ldots, n_B. \tag{1.95}$$

In the microscopic many-body system treated in Chapter 2, the commutator of $\underset{\sim}{H}$ and $\underset{\sim}{B}$ is calculated with the operators restricted to the model space. The reasons are explained there. We will do the same here and define $\dot{\underset{\sim}{B}}$ in matrix form as

$$\dot{\mathsf{B}} = \frac{i}{\hbar}(\mathsf{H} \cdot \mathsf{O} \cdot \mathsf{B} - \mathsf{B} \cdot \mathsf{O} \cdot \mathsf{H}), \tag{1.96}$$

as explained in Sec. 1.6.2.

1.6.5 Limitations of the representation and possible improvements

Whenever the state we want to represent does not vanish at the boundaries of the Hilbert space, the relative distance representation will be poor at the boundaries. This makes it necessary to use a more extended Hilbert space to avoid border effects. Thus, the matrices now need to run over $i, j = 0, \ldots, n + n_B + M$. This is important not only for the state, but also for the operators in the restricted Hilbert space. These operators correlate the

coefficients in $\vec{\Psi}$ in the boundary condition equations and thus they need to be well defined up to r_{n+n_B}. Therefore a bigger space is again the solution to this drawback.

Moreover, since the localized states display the oscillations visible in Fig. (1.23), these states have a broader extension than those forming the basis, so either the number of boundary condition equations can be expected to increase for good convergence of the result, or the matching point must be selected further in (at a certain b_{n-m}), or a combination of both. To avoid this problem and to keep working in an $(n + n_B)$-dimensional space, boundary conditions might be applied to the operators in the same way.

1.7 Boundary conditions in the discrete relative distance representation

To treat a problem as close as possible to the one in FMD, we will not make explicit use of the coordinate space representation of the gaussians, but rather the matrix elements of $\underset{\sim}{B} = \sqrt{\underset{\sim}{\vec{r}^{\,2}}}$. In this case, the procedure is exactly equivalent to the previous one, but the representation of the wave function and its derivatives is given in the way described in the previous section. The trial state remains as in Sec. 1.5.

In addition to the concerns of the previous section, it must be noted that the representation of $\underset{\sim}{B}$ in terms of the matrix elements for a gaussian set must cover and describe the trial state with enough accuracy. This implies that the set of gaussians must cover the space where the state is defined, with the same argument about negligible overlaps and expectation values we expounded previously.

1.7.1 Coulomb wave

The discrete relative distance representation is also able to represent a resonance, even though its wave function is non-zero at the boundary (see Fig. (1.26)). As figure (1.27) shows, to achieve this, more boundary conditions are needed as well as a larger Hilbert space and the boundary conditions must be applied at $R = b_{n-m} < b_n$. The accuracy of the results for the resonance parameters, shown in Table (1.5) is again excellent and they agree with the previous values, the same is true for the phase shift values (see Fig. (1.28)). Nevertheless, the precision of this approach is more limited, since the relative coordinate representation is an approximation and it fails to represent the $\ell = 4$ resonance with the same accuracy as the two previous representations. The result converges to one of the

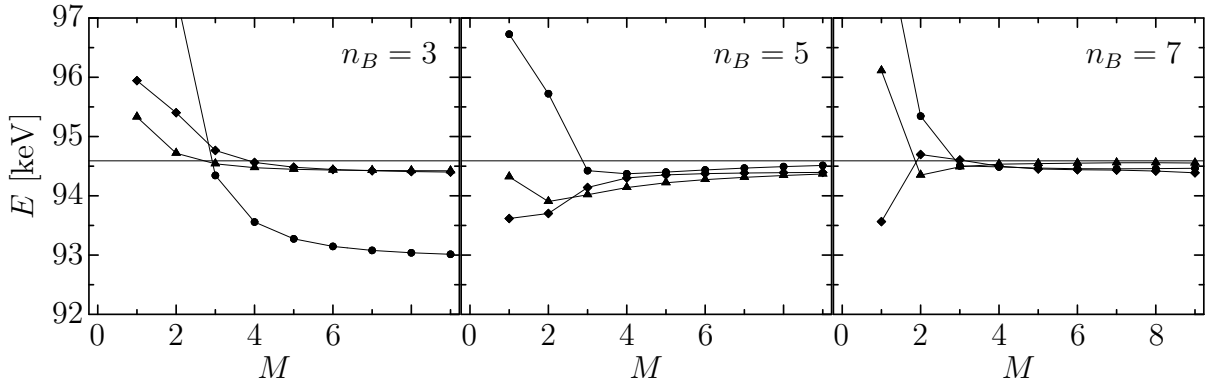

Figure 1.27: α-α system for $\ell = 0$. Convergence of energy and width with the extra M states for the discrete relative distance representation. Circles, diamonds and triangles correspond to $m = 0, 4$ and 8, respectively.

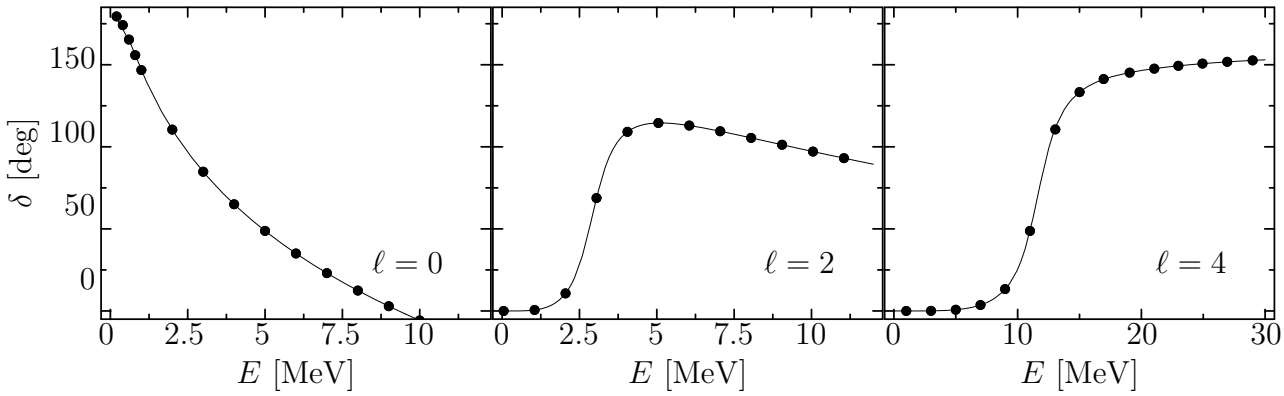

Figure 1.28: The circles depict the phase shifts for the α-α system calculated in a gaussian basis with the discrete relative distance representation. The solid lines represent the reference calculation with the grid method.

grid representations with the use of a smaller Δ_g (keeping constant the ratio a/Δ_g^2), but the quoted figures in this section have been calculated with the same basis as in the exact gaussian representation.

The relative distance representation can be made more accurate by considering a wider range of values of r. However, this would require a matching at larger distances and consequently converge to a higher eigenvalue, since the described wave function would display one oscillation or more. Since the dimensions of the matrices are typically 20×20, only the first few eigenvalues have enough accuracy, thus limiting the solution.

	$\ell = 0$		$\ell = 2$		$\ell = 4$	
	E [MeV]	Γ [eV]	E [MeV]	Γ [MeV]	E [MeV]	Γ [MeV]
Gamov Vector	0.0946	7.92	2.90	1.28	11.6	2.92

Table 1.5: Resonance parameters for an α-α system calculated with a gaussian basis in the discrete relative distance representation.

1.7.2 Free spherical wave

In this case, the limitations of the numerical integrals do not allow for a reliable calculation. The best values achieved for the resonance parameters are displayed in Table (1.6). The parameters n_B, m and M cannot take values that assure the convergence of the method, due to precision loss in the numerical integrals. This causes a higher deviation from the reference figures.

	$p_{3/2}$		$p_{1/2}$	
	E [MeV]	Γ [eV]	E [MeV]	Γ [MeV]
Gamov Vector	0.907	0.603	3.08	4.82

Table 1.6: Resonance parameters for the n-α system calculated with a gaussian basis in the discrete relative distance representation.

Chapter 2

*M*icroscopic Model

2.1 The nuclear model

2.1.1 Variational principle

In physics, variational principles not only generate the exact equations of motion but also lead to powerful approximations. One good starting point is the *Ritz Variational Principle*, which can be formulated as (see for example [10]):

The expectation value of the energy $E[Q]$, for a state $\left|\, Q \,\right\rangle$, for a given Hamiltonian $\underset{\sim}{H}$, is given by:

$$E[Q] = \frac{\left\langle\, Q \,\right| \underset{\sim}{H} \left|\, Q \,\right\rangle}{\left\langle\, Q \,\right| \left. Q \,\right\rangle}. \tag{2.1}$$

Any state which makes $E[Q]$ stationary whilst $\left|\, Q \,\right\rangle$ is varied over the whole Hilbert space is an eigenstate of $\underset{\sim}{H}$ with eigenvalue E.

This can be shown by taking a variation of either $\left|\, Q \,\right\rangle$ or $\left\langle\, Q \,\right|$:

$$\frac{\delta E[Q]}{\delta \left\langle\, Q \,\right|} = \frac{\left\langle\, \delta Q \,\right| \underset{\sim}{H} \left|\, Q \,\right\rangle}{\left\langle\, Q \,\right| \left. Q \,\right\rangle} - \frac{\left\langle\, Q \,\right| \underset{\sim}{H} \left|\, Q \,\right\rangle}{\left\langle\, Q \,\right| \left. Q \,\right\rangle^2} \left\langle\, \delta Q \,\right| \left. Q \,\right\rangle. \tag{2.2}$$

Demanding $E[Q]$ to be stationary results in:

$$\left\langle\, \delta Q \,\right| \underset{\sim}{H} \left|\, Q \,\right\rangle = \frac{\left\langle\, Q \,\right| \underset{\sim}{H} \left|\, Q \,\right\rangle}{\left\langle\, Q \,\right| \left. Q \,\right\rangle} \left\langle\, \delta Q \,\right| \left. Q \,\right\rangle. \tag{2.3}$$

Provided that $\langle \delta Q|$ is the most general variation possible, the eigenvalue problem is obtained:

$$\underset{\sim}{H} \left|\, Q \,\right\rangle = \frac{\left\langle\, Q \,\right| \underset{\sim}{H} \left|\, Q \,\right\rangle}{\left\langle\, Q \,\right| \left. Q \,\right\rangle} \left|\, Q \,\right\rangle. \tag{2.4}$$

$E[Q]$ is the eigenvalue of the corresponding state $\left|\, Q \,\right\rangle$ where the energy functional is stationary.

Since $\underset{\sim}{H}$ has a lower bound E_0, the value of the energy $E[Q]$ is always larger than or equal to E_0. The equality $E[Q] = E_0$ implies that $\big|\, Q \,\big\rangle$ is the ground state. Looking for the absolute minimum of $E[Q]$ within a restricted variational space leads to an approximation of the actual ground state.

It should be noted that for the most general variation $\big\langle\, \delta Q \,\big|$, all stationary points are saddle-points except for the ground state, which corresponds to the absolute minimum. If $\underset{\sim}{H}$ also has an upper bound the largest eigenvalue corresponds to the absolute maximum.

2.1.2 Hartree-Fock approximation

The Hartree-Fock approximation is one example of the variational principle that is often used. For identical fermions the trial state is a single Slater determinant

$$\begin{aligned} \big|\, Q \,\big\rangle &= \underset{\sim}{\mathcal{A}}\big(\big|\, q_1 \,\big\rangle \otimes \big|\, q_2 \,\big\rangle \otimes \ldots \otimes \big|\, q_A \,\big\rangle\big) \\ &= \frac{1}{A!} \sum_{\mathcal{P}} (-1)^{\mathcal{P}} \, \big(\big|\, q_{\mathcal{P}(1)} \,\big\rangle \otimes \big|\, q_{\mathcal{P}(2)} \,\big\rangle \otimes \ldots \otimes \big|\, q_{\mathcal{P}(A)} \,\big\rangle\big) \end{aligned} \tag{2.5}$$

which is built from orthogonal single-particle states that represent the variational degrees of freedom. The sum runs over all permutations $\mathcal{P}$.

The energy $E[\rho]$ of a single Slater determinant is uniquely given by the single-particle density ρ

$$\rho_{ij} = \big\langle\, Q \,\big|\, \underset{\sim}{a}_j^\dagger \underset{\sim}{a}_i \,\big|\, Q \,\big\rangle, \tag{2.6}$$

which is associated with the state $\big|\, Q \,\big\rangle$. $\underset{\sim}{a}_j^\dagger$ denotes the creation operator of a particle in the state labeled by j.

The energy is varied with respect to ρ under the constraint[1] that $\rho = \rho^2$,

$$\delta \Big[E[\rho] - \mathrm{Tr}\Big(\Lambda(\rho^2 - \rho)\Big)\Big] = 0. \tag{2.7}$$

Λ is the matrix of Lagrange multipliers that are needed to introduce the constraint $\rho = \rho^2$.

With some manipulations, this results in the Hartree-Fock equation:

$$[h[\rho], \rho] = h[\rho] \; \rho - \rho \; h[\rho] = 0, \tag{2.8}$$

where $h[\rho]$ represents the Hartree-Fock Hamiltonian given by

$$h[\rho] = \sum_{i,j=1}^{A} \big|\, q_i \,\big\rangle h_{ij}[\rho] \big\langle\, q_j \,\big|, \quad h_{ij}[\rho] = \frac{\delta E[\rho]}{\delta \rho_{ji}}. \tag{2.9}$$

The result is an independent-particle model, where each particle feels a mean field created by all the others. The Hartree-Fock equation (2.8) has to be solved by iterative

[1] This constraint is equivalent to saying that the total antisymmetric state $\big|\, Q \,\big\rangle$ is a Slater determinant.

methods, since $h[\rho]$ depends in a self-consistent way on ρ. Starting with an initial estimate of the states $\{\,|\,q_i\,\rangle\}$, ρ can be constructed; this allows us to calculate the corresponding h, then find its eigenvectors $\{\,|\,q_i\,\rangle\}$, which again yield a new ρ and so on until convergence is achieved.

The calculations can be done by representing the single-particle states for example on a grid in coordinate space, or by an expansion in an orthogonal basis (eigenstates of a harmonic oscillator, Wood-Saxon potential, etc.).

2.1.3 Fermionic Molecular Dynamics representation

In the Hartree-Fock method the single-particle states $|\,q_k\,\rangle$ are of the most general form. In practice however, their degrees of freedom are restricted, for example only a limited number of basis states are considered or the states are assumed to be axially symmetric.

In Fermionic Molecular Dynamics (FMD) [11] the single-particle state is the Kronecker product

$$|\,q_k\,\rangle = |\,a_k, \vec{b}_k\,\rangle \otimes |\,\chi_k\,\rangle \otimes |\,\xi_k\,\rangle, \tag{2.10}$$

where $|\,a_k, \vec{b}_k\,\rangle$ is the spatial part, $|\,\chi_k\,\rangle$ is the spin part, and $|\,\xi_k\,\rangle$ is the isospin part.

The spatial ket $|\,a_k, \vec{b}_k\,\rangle$ is a gaussian in coordinate space representation:

$$\langle\,\vec{x}\,|\,a_k, \vec{b}_k\,\rangle = \exp\left\{-\frac{(\vec{x}-\vec{b}_k)^2}{2a_k}\right\}. \tag{2.11}$$

The complex parameters $\vec{b_k} = \vec{r}_k + ia_k\,\vec{p}_k$ and a_k determine the mean position $\vec{r}_k$, mean momentum $\vec{p}_k$ and the width in both position and momentum:

$$\begin{aligned}
\vec{r}_k =& \frac{\langle\, a_k, \vec{b}_k \,|\, \underset{\sim}{\vec{x}} \,|\, a_k, \vec{b}_k\,\rangle}{\langle\, a_k, \vec{b}_k \,|\, a_k, \vec{b}_k\,\rangle} \qquad \vec{p}_k = \frac{\langle\, a_k, \vec{b}_k \,|\, \underset{\sim}{\vec{k}} \,|\, a_k, \vec{b}_k\,\rangle}{\langle\, a_k, \vec{b}_k \,|\, a_k, \vec{b}_k\,\rangle} \\
\frac{3}{2\,\mathrm{Re}\{a_k\}} =& \frac{\langle\, a_k, \vec{b}_k \,|\, (\underset{\sim}{\vec{k}} - \vec{p}_k)^2 \,|\, a_k, \vec{b}_k\,\rangle}{\langle\, a_k, \vec{b}_k \,|\, a_k, \vec{b}_k\,\rangle} \\
\frac{3}{2}\frac{\mathrm{Re}\{a_k\}^2 + \mathrm{Im}\{a_k\}^2}{\mathrm{Re}\{a_k\}} =& \frac{\langle\, a_k, \vec{b}_k \,|\, (\underset{\sim}{\vec{x}} - \vec{r}_k)^2 \,|\, a_k, \vec{b}_k\,\rangle}{\langle\, a_k, \vec{b}_k \,|\, a_k, \vec{b}_k\,\rangle},
\end{aligned} \tag{2.12}$$

where Im and Re denote the imaginary and real part of the parameters, respectively. In the many-body system this semiclassical picture is lost for overlapping states, due to antisymmetrization.

In spin space the most general state for spin $\frac{1}{2}$

$$|\,\chi_k\,\rangle = c_\uparrow |\uparrow\rangle + c_\downarrow |\downarrow\rangle, \tag{2.13}$$

is used. $|\uparrow\rangle$ and $|\downarrow\rangle$ are eigenstates of $\underset{\sim}{s}_z$.

In isospin space the nucleon is considered to be either a proton $\left|\, p \,\right\rangle$ or a neutron $\left|\, n \,\right\rangle$:

$$\left|\, \xi_k \,\right\rangle \in \left\{ \left|\, p \,\right\rangle, \left|\, n \,\right\rangle \right\}. \tag{2.14}$$

These states are orthonormal and have $\pm\frac{1}{2}$ as the eigenvalues of the third component of isospin.

2.1.4 Nucleon-nucleon interaction

When performing a Hartree-Fock calculation in nuclear physics, one is faced with two problems. The first is the representation of the single-particle states that compose the Slater determinant. Here it has been shown that the gaussian states used in FMD (see Sec. 2.1.3) are especially well suited for deformed nuclei. The second problem is the choice of an effective Hamiltonian. For testing purposes, a simple Volkov interaction will be used, while the final calculations will be performed with Bonn or Argonne realistic potentials. These are NN interactions based on meson exchange. They are realistic in the sense that their free parameters are adjusted in order to reproduce the NN scattering data and the deuteron properties [12].

The Slater determinants are not able to describe short-range correlations induced by realistic interactions. Therefore the Unitary Correlation Operator Method (UCOM) [13] is used. It defines an operator $\underset{\sim}{C}$ which when applied to the trial state $\left|\, Q \,\right\rangle$ implements short-range radial and tensor correlations. The result is a correlated many-body state

$$\left|\, \hat{Q} \,\right\rangle = \underset{\sim}{C} \left|\, Q \,\right\rangle \tag{2.15}$$

which by construction includes short-range correlations.

For convenience, the actual implementation of the correlator is done on the operators. Since $\underset{\sim}{C}$ is unitary, the method is equivalent to the one given above. For example, a correlated Hamiltonian is defined as

$$\underset{\sim}{\hat{H}} = \underset{\sim}{C}^{\dagger} \underset{\sim}{H} \underset{\sim}{C} \tag{2.16}$$

such that $\underset{\sim}{\hat{H}}$ can be used with the uncorrelated trial states $\left|\, Q \,\right\rangle$.

Equation (2.16) can be expanded into a series of contributions from one-body up to n-body operators:

$$\underset{\sim}{\hat{H}} = \underset{\sim}{\hat{H}}^{[1]} + \underset{\sim}{\hat{H}}^{[2]} + ... = \underset{\sim}{T} + \underset{\sim}{\hat{H}}^{[2]} + ..., \tag{2.17}$$

where the one-body part is only the kinetic energy and the two-body part has both kinetic and potential energy contributions.

Only the one-body and two-body contributions of the correlated interaction are used explicitly. The effect of the higher order contributions, as well as the effect of the genuine three-body forces, is simulated by a correction term $\underset{\sim}{\hat{H}}_{corr}$. This has been adjusted to reproduce the experimental binding energies and radii of the doubly-magic nuclei ^{4}He, ^{16}O and ^{40}Ca. The Coulomb interaction is also included:

$$\underset{\sim}{\hat{H}}_{eff} = \underset{\sim}{\hat{H}}^{[1]} + \underset{\sim}{\hat{H}}^{[2]} + ... = \underset{\sim}{T} + \underset{\sim}{\hat{H}}^{[2]} + \underset{\sim}{\hat{H}}_{corr}. \tag{2.18}$$

2.1.5 Multi-configuration calculations

For a more detailed and more precise description of nuclear structure, one has to go beyond the Hartree-Fock approximation and represent the many-body trial state by a linear combination of Slater determinants [14]. This method is called multi-configuration mixing.

We consider a Hilbert space formed by a set of nonorthogonal but linearly independent Slater determinants $\{\,|\,Q_i\,\rangle;\ i=1,\ldots,n+n_B\}$. The eigenstates of the Hamiltonian possess good spin and parity $J^\pi M$. Therefore the Slater determinants $|\,Q_i\,\rangle$ are projected on spin and parity

$$|\,J^\pi MK;\,Q_i\,\rangle = \underset{\sim}{P}{}^{J^\pi}_{MK}|\,Q_i\,\rangle. \tag{2.19}$$

Thus we obtain a subspace of the many-body Hilbert space spanned by the nonorthogonal states $|\,J^\pi MK;\,Q_i\,\rangle$, which all have the same spin J, parity π and magnetic quantum number M.

The Hamiltonian is then diagonalized in this subspace for each J^π:

$$\begin{aligned}\sum_{j=1}^{n+n_B}\sum_{K'=-J}^{J}\langle\,J^\pi MK;\,Q_i\,|\,\underset{\sim}{H}\,|\,J^\pi MK';\,Q_j\,\rangle\;\Psi^{\alpha J^\pi}_{jK'} = \\ = E^{J^\pi}_\alpha\sum_{j=1}^{n+n_B}\sum_{K'=-J}^{J}\langle\,J^\pi MK;\,Q_i\,|\,J^\pi MK';\,Q_j\,\rangle\;\Psi^{\alpha J^\pi}_{jK'},\end{aligned} \tag{2.20}$$

hence one obtains the eigenvalues $E^{J\pi}_\alpha$ and the corresponding eigenstates

$$|\,\Psi^{J^\pi M}_{E_\alpha}\,\rangle = \sum_{j=1}^{n+n_B}\sum_{K'=-J}^{J}\Psi^{\alpha J^\pi}_{jK'}|\,J^\pi MK';\,Q_j\,\rangle. \tag{2.21}$$

As the Hamiltonian commutes with $\underset{\sim}{P}{}^{J^\pi}_{MK}$ Eq. (2.20) can also be written as

$$\sum_{j=1}^{n+n_B}\sum_{K'=-J}^{J}\langle\,Q_i\,|\,\underset{\sim}{H}\underset{\sim}{P}{}^{J^\pi}_{MK'}\,|\,Q_j\,\rangle\;\Psi^{\alpha J^\pi}_{jK'} = E^{J^\pi}_\alpha\sum_{j=1}^{n+n_B}\sum_{K'=-J}^{J}\langle\,Q_i\,|\,\underset{\sim}{P}{}^{J^\pi}_{MK'}\,|\,Q_j\,\rangle\;\Psi^{\alpha J^\pi}_{jK'}. \tag{2.22}$$

If the states $|\,Q_j\,\rangle$ possess axial symmetry the summation over K' is not needed and we set $K=K'=M$. The α-α system has axial symmetry about the axis joining the two α-particles. In the n-α case we choose (without the loss of generality) the spin of the neutron to point in the direction of the axis joining the α-particle and the centroid of the gaussian for the neutron, so that this system also has axial symmetry up to a phase. For axial symmetry there is only one numerical integration to be performed when applying $\underset{\sim}{P}{}^{J^\pi}_{MM}$ so the numerical effort simplifies considerably and we are left with

$$\sum_{j=1}^{n+n_B}\langle\,Q_i\,|\,\underset{\sim}{H}\underset{\sim}{P}{}^{J^\pi}_{MM}\,|\,Q_j\,\rangle\;\Psi^{\alpha J^\pi}_{jM} = E^{J^\pi}_\alpha\sum_{j=1}^{n+n_B}\langle\,Q_i\,|\,\underset{\sim}{P}{}^{J^\pi}_{MM}\,|\,Q_j\,\rangle\;\Psi^{\alpha J^\pi}_{jM}. \tag{2.23}$$

For further information on the projection formalism see [15].

2.2 Collective-coordinate representation

The Slater determinants built from the FMD single-particle basis in general do not allow for an exact separation of the state into the different contributions as expressed in Eq. (1). Therefore we propose a collective-coordinate representation for the relative motion between the fragments. In the asymptotic limit the internal degrees of freedom are frozen inside the fragments and the many-body states (2.19) are of the form

$$\left| J^\pi MK;\, Q_i \right\rangle = \underset{\sim}{P}^{J^\pi}_{MK}\, \underset{\sim}{\mathcal{A}}\{ \left| Q_{\mathrm{C1}}; \vec{D}_{1i} \right\rangle \otimes \left| Q_{\mathrm{C2}}; \vec{D}_{2i} \right\rangle \}, \tag{2.24}$$

where $\vec{D}_{1i} = \frac{A_2}{A} D_i \vec{e}_z$ and $\vec{D}_{2i} = -\frac{A_1}{A} D_i \vec{e}_z$ denote the positions of the centers of the two clusters on the z-axis. The grid of distances D_i corresponds to the grid d_i in Sec. (1.5). In the following we will use the projected many-body states (2.24) not only in the asymptotic region, but also for small values of D. One could improve the Hilbert space by adding states which are obtained by minimizing the energy under constraints (adiabatic states). This will be a subject for future research.

In order to impose the boundary conditions on the many-body state, an operator defining a relative distance is needed. As discussed in Sec. 1.6, the indistinguishability of the particles in the many-body system does not allow for a straightforward definition of a relative distance operator. In the following subsections we will show that the operator $\underset{\sim}{B} = \frac{1}{A^2} \sum_{i<j=1}^{A} (\underset{\sim}{\vec{x}}(i) - \underset{\sim}{\vec{x}}(j))^2$, which is the mean square radius, is well suited as a distance measure.

2.2.1 Decomposition of operators

Let us consider a situation where a cluster C1 made up of A_1 identical particles, is localized in a spatial region $\mathcal{S}_1$ and a cluster C2 consisting of A_2 particles, is localized in a region $\mathcal{S}_2$ that has no overlap with $\mathcal{S}_1$ ($\mathcal{S}_1 \cap \mathcal{S}_2 = \emptyset$). In that case, the identical particles in C1 can be distinguished from those in C2 by their different locations. The particles within C1 cannot be distinguished from each other and the same holds for those within C2. In such a situation antisymmetrization is only required among the particles of each cluster. For calculating expectation values, the state

$$\underset{\sim}{\mathcal{A}}\Big(\left| \Psi_{\mathrm{C1}} \right\rangle \otimes \left| \Psi_{\mathrm{C2}} \right\rangle \Big) \tag{2.25}$$

gives the same result as

$$\Big(\underset{\sim}{\mathcal{A}} \left| \Psi_{\mathrm{C1}} \right\rangle \Big) \otimes \Big(\underset{\sim}{\mathcal{A}} \left| \Psi_{\mathrm{C2}} \right\rangle \Big). \tag{2.26}$$

Therefore, it is meaningful to express the operators related to the problem as a sum of different contributions. The labels corresponding to each of the fragments can be grouped as $I_1 = \{1, 2, \ldots, A_1\}$ for the first cluster and $I_2 = \{A_1 + 1, \ldots, A_1 + A_2 = A\}$ for the second one. With this it is possible to define the total momentum of each fragment,

$$\underset{\sim}{\vec{K}}_1 = \sum_{i \in I_1} \underset{\sim}{\vec{k}}(i), \quad \underset{\sim}{\vec{K}}_2 = \sum_{i \in I_2} \underset{\sim}{\vec{k}}(i), \tag{2.27}$$

as well as the intrinsic momentum of each particle with respect to the fragment it belongs to,

$$\underset{\sim}{\vec{\kappa}}(a,i) = \underset{\sim}{\vec{k}}(i) - \frac{1}{A_a}\underset{\sim}{\vec{K}}_a, \quad i \in I_a, \quad a = 1,2. \tag{2.28}$$

For simplicity we assume an equal mass of m for all nucleons. It is important to note that

$$\sum_{i\in I_a} \underset{\sim}{\vec{\kappa}}(a,i) = 0, \quad a = 1,2. \tag{2.29}$$

The total kinetic energy can be then decomposed into four contributions:

$$\begin{aligned} \underset{\sim}{T} = \frac{1}{2m}\sum_{i=1}^{A} \underset{\sim}{\vec{k}}^2(i) &= \underset{\sim}{T}_{rel} + \underset{\sim}{T}_1 + \underset{\sim}{T}_2 + \underset{\sim}{T}_{CM} \\ &= \frac{1}{2\mu}\underset{\sim}{\vec{K}}^2 + \frac{1}{2m}\sum_{i\in I_1}\underset{\sim}{\vec{\kappa}}^2(a,i) + \frac{1}{2m}\sum_{j\in I_2}\underset{\sim}{\vec{\kappa}}^2(a,j) + \frac{1}{2Am}\underset{\sim}{\vec{K}}^2_{CM}, \end{aligned} \tag{2.30}$$

The first term is the kinetic energy in the relative motion, with

$$\underset{\sim}{\vec{K}} = \frac{A_2}{A}\underset{\sim}{\vec{K}}_1 - \frac{A_1}{A}\underset{\sim}{\vec{K}}_2. \tag{2.31}$$

$\mu = mA_1A_2/A$ is the reduced mass of the system. The second and third terms are the intrinsic energy of the fragments C1 and C2, which depend only on the internal degrees of freedom of the fragments and the last term is the center of mass kinetic energy:

$$\underset{\sim}{\vec{K}}_{CM} = \underset{\sim}{\vec{K}}_1 + \underset{\sim}{\vec{K}}_2. \tag{2.32}$$

An analogous separation can be made for an operator that will be used to define the relative distance between the clusters. We start with an operator that depends on the relative distance between the nucleons and is symmetric with respect to particle exchange:

$$\underset{\sim}{B} = \sum_{i>j}^{A} g((\underset{\sim}{\vec{x}}(i) - \underset{\sim}{\vec{x}}(j))^2). \tag{2.33}$$

If we define the relative position with respect to the center of mass of each cluster as:

$$\underset{\sim}{\vec{\xi}}(a,i) = \underset{\sim}{\vec{x}}(i) - \underset{\sim}{\vec{X}}_a, \quad i \in I_a, \quad a = 1,2 \quad , \tag{2.34}$$

where

$$\underset{\sim}{\vec{X}}_a = \frac{1}{A_a}\sum_{i\in I_a}\underset{\sim}{\vec{x}}(i), \tag{2.35}$$

then $\underset{\sim}{B}$ can be written as

$$\begin{aligned} \underset{\sim}{B} = \underset{\sim}{B}_{rel} + \underset{\sim}{B}_1 + \underset{\sim}{B}_2 =& 2\sum_{i\in I_1}\sum_{j\in I_2} g((\underset{\sim}{\vec{X}} + \underset{\sim}{\vec{\xi}}(1,i) - \underset{\sim}{\vec{\xi}}(2,j))^2) \\ &+ \sum_{i,j\in I_1} g((\underset{\sim}{\vec{\xi}}(1,i) - \underset{\sim}{\vec{\xi}}(1,j))^2) + \sum_{i,j\in I_2} g((\underset{\sim}{\vec{\xi}}(2,i) - \underset{\sim}{\vec{\xi}}(2,j))^2). \end{aligned} \tag{2.36}$$

$\underset{\sim}{\vec{X}}$ is the relative distance between the centers of mass of the fragments,

$$\underset{\sim}{\vec{X}} = \underset{\sim}{\vec{X}}_1 - \underset{\sim}{\vec{X}}_2 \tag{2.37}$$

and

$$\frac{1}{A}\sum_{i=1}^{A} \underset{\sim}{\vec{x}}(i) = \underset{\sim}{\vec{X}}_{CM} = (A_1 \underset{\sim}{\vec{X}}_1 + A_2 \underset{\sim}{\vec{X}}_2)/A \tag{2.38}$$

is the center of mass of the whole system. Note that

$$\sum_{i\in I_a} \underset{\sim}{\vec{\xi}}(a,i) = 0, \quad a = 1,2. \tag{2.39}$$

Asymptotically (when the two fragments are far from each other), the mean value of $|\underset{\sim}{\vec{X}}|$ is much greater than that of $|\underset{\sim}{\vec{\xi}}(1,i)|$ or $|\underset{\sim}{\vec{\xi}}(2,j)|$ and the latter can be neglected in the first term of Eq. (2.36). Thus, asymptotically, $\underset{\sim}{B}$ splits up into three terms that depend on the relative distance between the fragments and the internal degrees of freedom of the two clusters.

The decomposition is exact if we use $g((\underset{\sim}{\vec{x}}(i) - \underset{\sim}{\vec{x}}(j))^2) = \frac{1}{A^2}(\underset{\sim}{\vec{x}}(i) - \underset{\sim}{\vec{x}}(j))$. $\underset{\sim}{B}$ is then just the mean square radius:

$$\begin{aligned}
\underset{\sim}{B} =& \frac{1}{A}\sum_{i=1}^{A}(\underset{\sim}{\vec{x}}(i) - \underset{\sim}{\vec{X}}_{CM})^2 = \frac{1}{A^2}\sum_{i<j=1}^{A}(\underset{\sim}{\vec{x}}(i) - \underset{\sim}{\vec{x}}(j))^2 \\
=& \frac{\mu_A}{A}\,\underset{\sim}{\vec{X}}^2 + \frac{1}{A}\sum_{i\in I_1}(\underset{\sim}{\vec{\xi}}(1,i))^2 + \frac{1}{A}\sum_{j\in I_2}(\underset{\sim}{\vec{\xi}}(2,j))^2 \\
=& \underset{\sim}{B}_{rel} + \underset{\sim}{B}_1 + \underset{\sim}{B}_2,
\end{aligned} \tag{2.40}$$

where $\mu_A = \mu/m$.

It is important to point out that the quantum mechanically correct observables, which are symmetric under particle permutations, are $\underset{\sim}{B}$ and $\underset{\sim}{T}$. Hence, only expectation values of these observables are meaningful within the antisymmetrized many-body basis. Using $\underset{\sim}{B}_{rel}$, $\underset{\sim}{T}_{rel}$ or $\underset{\sim}{\vec{X}}$, $\underset{\sim}{\vec{K}}$ alone, is not possible as they are not symmetric under particle exchange; for example $\left\langle \Psi \right| \underset{\sim}{\mathcal{A}}\underset{\sim}{\vec{K}}\underset{\sim}{\mathcal{A}} \left| \Psi \right\rangle = 0$ and $\left\langle \Psi \right| \underset{\sim}{\mathcal{A}}\underset{\sim}{\vec{X}}\underset{\sim}{\mathcal{A}} \left| \Psi \right\rangle = 0$ for any state $\left| \Psi \right\rangle$.

2.2.2 Commutation relations and eigenrepresentation

It is straightfoward to show that the following properties are fulfilled by the operators for collective coordinates defined in the previous section:

$$\begin{aligned}
\left[\underset{\sim}{X}^{(i)}, \underset{\sim}{K}^{(j)}\right] &= i\hbar\delta_{ij}, \\
\left[\underset{\sim}{X}_a^{(i)}, \underset{\sim}{K}_a^{(j)}\right] &= i\hbar\delta_{ij}, \quad a = 1,2, \quad i,j = x,y,z \\
\left[\underset{\sim}{X}_{CM}^{(i)}, \underset{\sim}{K}_{CM}^{(j)}\right] &= i\hbar\delta_{ij}.
\end{aligned} \tag{2.41}$$

Hence, $\vec{\underset{\sim}{K}}$ is the conjugate variable of $\vec{\underset{\sim}{X}}$, and analogously for the center of mass $\vec{\underset{\sim}{K}}_a$ and $\vec{\underset{\sim}{X}}_a$ of the first and second fragments, as well as for the total center of mass $\vec{\underset{\sim}{K}}_{CM}$ and $\vec{\underset{\sim}{X}}_{CM}$.

Moreover, operators for different collective types (the relative motion, center of mass of first and second fragment, total center of mass) commute:

$$\begin{aligned}
\left[\underset{\sim}{X}^{(i)}, \underset{\sim}{X}^{(j)}_{CM}\right] = 0, \quad \left[\underset{\sim}{K}^{(i)}, \underset{\sim}{K}^{(j)}_{CM}\right] = 0, \\
\left[\underset{\sim}{X}^{(i)}, \underset{\sim}{X}^{(j)}_{a}\right] = 0, \quad \left[\underset{\sim}{K}^{(i)}, \underset{\sim}{K}^{(j)}_{a}\right] = 0, \quad a = 1,2, \quad i,j = x,y,z \\
\left[\underset{\sim}{X}^{(i)}_{CM}, \underset{\sim}{X}^{(j)}_{a}\right] = 0, \quad \left[\underset{\sim}{K}^{(i)}_{CM}, \underset{\sim}{K}^{(j)}_{a}\right] = 0,
\end{aligned} \tag{2.42}$$

and

$$\begin{aligned}
\left[\underset{\sim}{X}^{(i)}, \underset{\sim}{K}^{(j)}_{CM}\right] = 0, \quad \left[\underset{\sim}{K}^{(i)}, \underset{\sim}{X}^{(j)}_{CM}\right] = 0, \\
\left[\underset{\sim}{X}^{(i)}, \underset{\sim}{K}^{(j)}_{a}\right] = 0, \quad \left[\underset{\sim}{K}^{(i)}, \underset{\sim}{X}^{(j)}_{a}\right] = 0, \quad a = 1,2, \quad i,j = x,y,z \\
\left[\underset{\sim}{X}^{(i)}_{CM}, \underset{\sim}{K}^{(j)}_{a}\right] = 0, \quad \left[\underset{\sim}{K}^{(i)}_{CM}, \underset{\sim}{X}^{(j)}_{a}\right] = 0.
\end{aligned} \tag{2.43}$$

From this we conclude that

$$\left[\underset{\sim}{B}_a, \vec{\underset{\sim}{B}}_{rel}\right] = 0, \quad \left[\underset{\sim}{B}_1, \underset{\sim}{B}_2\right] = 0, \quad a = 1,2 \tag{2.44}$$

and thus it is possible to define a common eigenrepresentation for the asymptotic region where the fragments do not overlap:

$$\begin{aligned}
\underset{\sim}{B}_{rel} \big| \, b_{rel}, \beta^{(1)}, \beta^{(2)}, \beta_{CM} \, \big\rangle &= b_{rel} \big| \, b_{rel}, \beta^{(1)}, \beta^{(2)}, \beta_{CM} \, \big\rangle \\
\underset{\sim}{B}_1 \big| \, b_{rel}, \beta^{(1)}, \beta^{(2)}, \beta_{CM} \, \big\rangle &= \beta^{(1)} \big| \, b_{rel}, \beta^{(1)}, \beta^{(2)}, \beta_{CM} \, \big\rangle \\
\underset{\sim}{B}_2 \big| \, b_{rel}, \beta^{(1)}, \beta^{(2)}, \beta_{CM} \, \big\rangle &= \beta^{(2)} \big| \, b_{rel}, \beta^{(1)}, \beta^{(2)}, \beta_{CM} \, \big\rangle \\
\vec{\underset{\sim}{X}}^2_{CM} \big| \, b_{rel}, \beta^{(1)}, \beta^{(2)}, \beta_{CM} \, \big\rangle &= \beta_{CM} \big| \, b_{rel}, \beta^{(1)}, \beta^{(2)}, \beta_{CM} \, \big\rangle.
\end{aligned} \tag{2.45}$$

It is also important to point out that in the asymptotic regime where total antisymmetrization is not needed anymore, the decomposition of $\underset{\sim}{B}$ in a sum of commuting contributions is in accordance with a direct product for the eigenstates,

$$\big| \, b_{rel}, \beta^{(1)}, \beta^{(2)}, \beta_{CM} \, \big\rangle = \big| \, b_{rel} \, \big\rangle \otimes \big| \, \beta^{(1)} \, \big\rangle \otimes \big| \, \beta^{(2)} \, \big\rangle \otimes \big| \, \beta_{CM} \, \big\rangle \tag{2.46}$$

and $\underset{\sim}{B} = \underset{\sim}{B}_{rel} + \underset{\sim}{B}_1 + \underset{\sim}{B}_2$ can be written, in the sense of

$$\underset{\sim}{B} = \underset{\sim}{B}_{rel} \otimes \underset{\sim}{1} \otimes \underset{\sim}{1} \otimes \underset{\sim}{1} + \underset{\sim}{1} \otimes \underset{\sim}{B}_1 \otimes \underset{\sim}{1} \otimes \underset{\sim}{1} + \underset{\sim}{1} \otimes \underset{\sim}{1} \otimes \underset{\sim}{B}_2 \otimes \underset{\sim}{1}. \tag{2.47}$$

Since a fragment is not an eigenstate of the square radius, the asymptotic states will not possess the good quantum numbers $\beta^{(1)}$ or $\beta^{(2)}$, but the relative motion still separates from the intrinsic one, so that states of the form

$$\big| \, b_{rel} \, \big\rangle \otimes \big| \, \mathrm{C1} \, \big\rangle \otimes \big| \, \mathrm{C2} \, \big\rangle \otimes \big| \, \Psi_{\mathrm{CM}} \, \big\rangle \tag{2.48}$$

will still be eigenstates of $\underset{\sim}{B}_{rel}$. For these types of states the expectation value of $\underset{\sim}{B}$ is

$$\begin{aligned}\big\langle\, b_{rel}\,\big|\otimes\big\langle\,\mathrm{C1}\,\big|\otimes\big\langle\,\mathrm{C2}\,\big|\otimes\big\langle\,\Psi_{\mathrm{CM}}\,\big|\;\underset{\sim}{B}\;\big|\,b_{rel}\,\big\rangle\otimes\big|\,\mathrm{C1}\,\big\rangle\otimes\big|\,\mathrm{C2}\,\big\rangle\otimes\big|\,\Psi_{\mathrm{CM}}\,\big\rangle \\ = b_{rel} + \big\langle\,\mathrm{C1}\,\big|\,\underset{\sim}{B}_1\,\big|\,\mathrm{C1}\,\big\rangle + \big\langle\,\mathrm{C2}\,\big|\,\underset{\sim}{B}_2\,\big|\,\mathrm{C2}\,\big\rangle,\end{aligned} \tag{2.49}$$

where $r^2_{\mathrm{C1}} = A\big\langle\,\mathrm{C1}\,\big|\,\underset{\sim}{B}_1\,\big|\,\mathrm{C1}\,\big\rangle/A_1$ and $r^2_{\mathrm{C2}} = A\big\langle\,\mathrm{C2}\,\big|\,\underset{\sim}{B}_2\,\big|\,\mathrm{C2}\,\big\rangle/A_2$ are the respective square radii of fragments C1 and C2 which are independent on b_{rel}. We conclude that the operator $\underset{\sim}{B}$ is a measure of the relative distance between the fragments in the asymptotic regime.

As the overlap between the clusters increases, the decomposition loses its meaning and so does the labeling in terms of their eigenvalues. However, $\underset{\sim}{B}$ is always a valid operator and its eigenvalues

$$b = b_{rel}(r) + \beta^{(1)} + \beta^{(2)} \tag{2.50}$$

can serve as a distance measure $b(r)$ as discussed in Sec. 1.6, even when the system does not have the cluster structure (2.24). Asymptotically the relation between b and the distance r between the fragments is well defined, namely

$$b(r) = \frac{\mu_A}{A}r^2 + \frac{A_1}{A}r^2_{\mathrm{C1}} + \frac{A_2}{A}r^2_{\mathrm{C2}}, \tag{2.51}$$

which follows from Eq. (2.40).

For simplicity we keep this relation as the definition for all values of b and can thus define the relative distance for arbitrary states as

$$r(b) = \sqrt{\Big(A\,b - A_1\,r^2_{\mathrm{C1}} - A_2\,r^2_{\mathrm{C2}}\Big)/\mu_A}, \tag{2.52}$$

as was already discussed in Sec. 1.6.1.

2.2.3 Collective-coordinate representation

The first step is to solve the eigenvalue problem for $\underset{\sim}{B}$,

$$\underset{\sim}{B}\;\big|\,b_t;\,J^\pi M\,\big\rangle = b_t^{J^\pi}\;\big|\,b_t;\,J^\pi M\,\big\rangle, \tag{2.53}$$

in the model space spanned by the projected FMD states $\{\big|\,J^\pi MK;\,Q_i\,\big\rangle;\;i=1,\ldots,n+n_B;\;K=-J,\ldots,J\}$. The orthonormalized eigenstates $\big|\,b_t;\,J^\pi M\,\big\rangle$ are localized states in the collective-coordinate representation; they are given in terms of $\big|\,J^\pi MK;\,Q_j\,\big\rangle$ as

$$\big|\,b_t;\,J^\pi M\,\big\rangle = \sum_{j,K'}\beta^{tJ^\pi}_{jK'}\big|\,J^\pi MK';\,Q_j\,\big\rangle. \tag{2.54}$$

For axially symmetric situations the sum over K' reduces to one term (for the α-α system, $K'=0$ and for the n-α sytem $K'=1/2$).

The diagonalization of $\underset{\sim}{B}$ in the basis defined by the set of projected FMD states, yields the coefficients $\beta^{tJ^\pi}_{jM}$:

$$\sum_{j=1}^{n+n_B} \left\langle Q_i \right| \underset{\sim}{B} \underset{\sim}{P}^{J^\pi}_{MM} \left| Q_j \right\rangle \beta^{tJ^\pi}_{jM} = b_t^{J^\pi} \sum_{j=1}^{n+n_B} \left\langle Q_i \right| \underset{\sim}{P}^{J^\pi}_{MM} \left| Q_j \right\rangle \beta^{tJ^\pi}_{jM}, \; i = 1, \ldots, n+n_B, \quad (2.55)$$

where we have already removed the sum in K' and set $K = K' = M$.

2.2.4 Relative wave function

With the collective-coordinate representation, we define the radial wave function of the relative motion at discrete values of the distance, as:

$$u_{kJ^\pi}(r(b_t)) = \mathcal{C} \; r(b_t) \big\langle \, b_t; \, J^\pi M \, \big| \, \Psi^{J^\pi M}_{E_\alpha} \, \big\rangle, \quad (2.56)$$

where $\left| \, \Psi^{J^\pi M}_{E_\alpha} \, \right\rangle$ is the eigenstate (2.21) of the Hamiltonian $\underset{\sim}{H}$ in the model space, and fulfils the desired boundary conditions. The relation (2.52) is used to relate the eigenvalues b_t of $\underset{\sim}{B}$, to the relative distance r.

As long as the projected FMD states that contribute to a certain localized state share the same intrinsic degrees of freedom for the fragments, the bra $\left\langle \, b_t; \, J^\pi M \right|$ applied on the trial state $\left| \, \Psi^{J^\pi M}_{E_\alpha} \, \right\rangle$ will represent the relative wave function at $r_t = r(b_t)$, because the internal degrees of freedom integrate out giving a constant and the corresponding relative distance can be extracted from the eigenvalue b_t. Note that the angular dependence also integrates out, as it is the same for all projected FMD states. The center of mass for the cases studied here, factorizes and is also the same for all configurations. For a more general case, a projection on the center of mass should also be included. All contributions that have been integrated are included in the constant $\mathcal{C}$.

In terms of the vectors $\vec{\beta}^{tJ^\pi}_M = \{\beta^{tJ^\pi}_{1M}, \beta^{tJ^\pi}_{2M}, \ldots\}$ and $\vec{\Psi}^{\alpha J^\pi}_M = \{ \, \Psi^{\alpha J^\pi}_{1M}, \; \Psi^{\alpha J^\pi}_{2M}, \ldots \}$ and by defining the overlap matrix

$$\mathsf{N}_{ij} = \left\langle \, J^\pi MM; \, Q_i \, \right| \left. J^\pi MM; \, Q_j \, \right\rangle, \quad (2.57)$$

one can write

$$u_{kJ^\pi}(r_t) = \mathcal{C} \; r(b_t) \; (\vec{\beta}^{tJ^\pi}_M)^\dagger \; \mathsf{N} \; \vec{\Psi}^{\alpha J^\pi}_M, \quad (2.58)$$

which is of the same form as described for the schematic model in Sec. 1.6.2, but where many-body states are now involved.

2.2.5 The relative velocity operator

The boundary condition equations involve not only $\underset{\sim}{B}$, but also powers of the velocity operator $\underset{\sim}{\dot{B}}$. In contrast to the schematic model, the operator $\underset{\sim}{B}$ also acts on the intrinsic degrees of freedom of the fragments. In the following we will show under which conditions

the intrinsic parts $\dot{\underset{\sim}{B}}_1$ and $\dot{\underset{\sim}{B}}_2$ do not contribute, in which case $\dot{\underset{\sim}{B}}$ can be regarded as the relative velocity.

In the neighbourhood of the matching point, where the fragments are already separated, the Hamiltonian can be decomposed as

$$\underset{\sim}{H} = (\underset{\sim}{T}_{rel} + \underset{\sim}{V}_{rel}) + \underset{\sim}{H}_1 + \underset{\sim}{H}_2, \tag{2.59}$$

where $\underset{\sim}{V}_{rel}$ is the mutual Coulomb energy of the fragments and $\underset{\sim}{H}_1$ and $\underset{\sim}{H}_2$ are the intrinsic Hamiltonians. Using the commutation relations derived in Sec. 2.2.2 and $[\underset{\sim}{B}_{rel}, \underset{\sim}{V}_{rel}] = 0$, the velocity operator assumes the following form in the asymptotic regime:

$$\begin{aligned} \dot{\underset{\sim}{B}} = \frac{i}{\hbar}\big[\underset{\sim}{H}, \underset{\sim}{B}\big] \quad &\xrightarrow[\text{distance}]{\text{large}} \quad \frac{i}{\hbar}\Big(\big[\underset{\sim}{T}_{rel}, \underset{\sim}{B}_{rel}\big] + \big[\underset{\sim}{H}_1, \underset{\sim}{B}_1\big] + \big[\underset{\sim}{H}_2, \underset{\sim}{B}_2\big]\Big) \\ &= \dot{\underset{\sim}{B}}_{rel} + \dot{\underset{\sim}{B}}_1 + \dot{\underset{\sim}{B}}_2. \end{aligned} \tag{2.60}$$

As long as we are calculating matrix elements of $\dot{\underset{\sim}{B}}$ with the asymptotic states (2.24) (as is done in Eq. (2.68)), with frozen states for fragments; the contribution from $\dot{\underset{\sim}{B}}_1$ is only from fragment C1 and can be written as the time derivative of the mean square radius:

$$\big\langle\, \mathrm{C1} \,\big|\, \dot{\underset{\sim}{B}} \,\big|\, \mathrm{C1} \,\big\rangle = \frac{d}{dt}\big\langle\, \mathrm{C1} \,\big|\, \underset{\sim}{B} \,\big|\, \mathrm{C1} \,\big\rangle \tag{2.61}$$

and the analogous equation applies for C2. As long as $\big|\, \mathrm{C1} \,\big\rangle$ and $\big|\, \mathrm{C2} \,\big\rangle$ are stationary in time, for example an eigenstate of $\underset{\sim}{H}_1$ or $\underset{\sim}{H}_2$, the contribution from the frozen fragments vanishes. The same arguments hold for higher powers of $\dot{\underset{\sim}{B}}$.

To summarize, whenever the intrinsic degrees of freedom in each fragment are frozen, only the relative velocity $\dot{\underset{\sim}{B}}_{rel}$ between the fragments contributes to the velocity $\dot{\underset{\sim}{B}}$.

2.2.6 Implementation of derivatives

"Derivatives" of the radial wave function (2.56) at the position $r_t = r(b_t)$ can be defined using the velocity operator $\dot{\underset{\sim}{B}}$ in complete analogy to Sec. 1.6.4 as

$$\big\langle\, b_t;\, J^\pi M \,\big|\, (\dot{\underset{\sim}{B}})^s \,\big|\, \Psi^{J^\pi M}_{E_\alpha} \,\big\rangle, \quad s = 1, 2, \dots \quad , \tag{2.62}$$

with the same proviso as before that the contributing FMD states have the structure (2.24) of frozen fragments. In the case of $\underset{\sim}{B} = 1/A^2 \sum_{i<j=1}^{A} (\vec{\underset{\sim}{x}}(i) - \vec{\underset{\sim}{x}}(j))^2$ in FMD and $\underset{\sim}{B} = \underset{\sim}{r}^2$ in the one-dimensional asymptotic region we can identify

$$r(b_t)\big\langle\, b_t;\, J^\pi M \,\big|\, \dot{\underset{\sim}{B}} \,\big|\, \Psi^{J^\pi M}_{E_\alpha} \,\big\rangle\, \mathcal{C} = \frac{-i\hbar}{4\mu}(u_{kJ^\pi}(r(b_t)) + 2r_t \frac{du_{kJ^\pi}}{dr}(r(b_t))). \tag{2.63}$$

The constant $\mathcal{C}$ is the same as in the definition of the wave function (2.56) because $\dot{\underset{\sim}{B}}$ and $\underset{\sim}{B}$ do not act on the integrated angular degrees of freedom.

The matrix element in this equation is calculated in the restricted model space in an manner analogous to Sec. 1.6.2. Therefore,

$$\left\langle\, b_t;\, J^\pi M \,\middle|\, \underset{\sim}{\dot{B}} \,\middle|\, \Psi_{E_\alpha}^{J^\pi M} \,\right\rangle = \sum_{i,j=1}^{n+n_B} (\beta_{iM}^{tJ^\pi})^*\ \Psi_{jM}^{\alpha J^\pi} \left\langle\, J^\pi MM;\, Q_i \,\middle|\, \underset{\sim}{\dot{B}} \,\middle|\, J^\pi MM;\, Q_j \,\right\rangle, \tag{2.64}$$

where the matrix elements of $\underset{\sim}{\dot{B}}$ in the basis $\left|\, J^\pi MM;\, Q_i \,\right\rangle$ are defined as $\dot{\mathsf{B}}_{ij}$ and calculated from

$$\dot{\mathsf{B}} = \frac{i}{\hbar}(\mathsf{H}\cdot\mathsf{O}\cdot\mathsf{B} - \mathsf{B}\cdot\mathsf{O}\cdot\mathsf{H}). \tag{2.65}$$

The matrices involved are defined in the same way as the overlaps in Sec. 2.2.4:

$$\begin{aligned} \mathsf{H}_{ij} &= \left\langle\, J^\pi MM;\, Q_i \,\middle|\, \underset{\sim}{H} \,\middle|\, J^\pi MM;\, Q_j \,\right\rangle \\ \mathsf{B}_{ij} &= \left\langle\, J^\pi MM;\, Q_i \,\middle|\, \underset{\sim}{B} \,\middle|\, J^\pi MM;\, Q_j \,\right\rangle \\ \mathsf{O}_{ij} &= (\mathsf{N}^{-1})_{ij}. \end{aligned} \tag{2.66}$$

Powers of the relative velocity many-body operator can be obtained in the restricted Hilbert space from

$$\begin{aligned} (\dot{\mathsf{B}})^2 &= \dot{\mathsf{B}}\cdot\mathsf{O}\cdot\dot{\mathsf{B}}, \\ (\dot{\mathsf{B}})^3 &= \dot{\mathsf{B}}\cdot\mathsf{O}\cdot\dot{\mathsf{B}}\cdot\mathsf{O}\cdot\dot{\mathsf{B}}, \\ &\vdots \end{aligned} \tag{2.67}$$

2.3 Formulation of boundary conditions

In the schematic model in Chapter 1, the relative distance was the genuine degree of freedom so there was no problem in matching the interior solution $u_{k\ell J}(r)$ to the Coulomb or free wave function $w_{k\ell J}(r)$ in the asymptotic region.

The many-body state consists of an antisymmetrized product of single-particle states and in general can not be separated into a center of mass part, a relative motion part and the internal degrees of freedom within the clusters. Therefore, in the previous section we defined an operator for the relative distance between the fragments and showed that in the asymptotic region it possesses the desired properties.

The eigenstates $\left| \, b_t;\, J^\pi M \, \right\rangle$ of $\underset{\sim}{B}$ are localized as much as possible within the restricted model space and thus play the same role as the localized states $\left| \, b_j \, \right\rangle$ did in the schematic model. Transferring the concepts of the schematic model in Sec. 1.6, which have proven to work successfully, to the FMD case; we are able to match the FMD many-body states to the simple asymptotic Coulomb or free waves $w_{k\ell J}(r)$ which have only one degree of freedom.

The wave function $u_{kJ^\pi}(r(b_t))$ and its derivatives, as defined in the previous section, make it possible to express the boundary conditions as

$$\frac{\left\langle \, b_t;\, J^\pi M \, \middle| \, (\underset{\sim}{\dot{B}})^s \, \middle| \, \Psi^{J^\pi M}_{E_\alpha} \, \right\rangle}{\left\langle \, b_t;\, J^\pi M \, \middle| \, \Psi^{J^\pi M}_{E_\alpha} \, \right\rangle} = \frac{\left\langle \, r(b_t) \, \middle| \, (\underset{\sim}{\dot{B}})^s \, \middle| \, w(k,\ell,J) \, \right\rangle}{\left\langle \, r(b_t) \, \middle| \, w(k,\ell,J) \, \right\rangle} := A^s_{k\ell J}, \quad s = 1, \ldots, n_B, \tag{2.68}$$

thus relating the microscopic many-body world to the one-dimensional asymptotic world. The $(\underset{\sim}{\dot{B}})^s$ in the matrix element on the right-hand side of this equation is the analogous to $\underset{\sim}{\dot{B}}_{rel}$, namely $(\underset{\sim}{p}\,\underset{\sim}{r} + \underset{\sim}{r}\,\underset{\sim}{p})/\mu$, see Eq. (1.90).

This equation can be rewritten in terms of the projected FMD basis ((2.24) or (2.19) in a more general case) as

$$\sum_{i,j=1}^{n+n_B} (\beta^{tJ^\pi}_{iM})^* \left(\left\langle \, J^\pi MM;\, Q_i \, \middle| \, (\underset{\sim}{\dot{B}})^s - A^s_{k\ell J} \, \middle| \, J^\pi MM;\, Q_j \, \right\rangle \right) \Psi^{\alpha J^\pi}_{jM} = 0, \quad s = 1, \ldots, n_B. \tag{2.69}$$

If we are not dealing with axially symmetric states, the basis is $\left| \, J^\pi MK;\, Q_i \, \right\rangle$ and an additional sum over K and K' has to be performed. Solving the resulting set of n_B equations, we obtain the equivalent of Eq. (1.53)

$$\Psi^{\alpha J^\pi}_{jM} = \sum_{i=1}^{n} s_{ij} \; \Psi^{\alpha J^\pi}_{iM}, \quad j = n+1, \ldots, n+n_B, \tag{2.70}$$

however the coefficients are now determined by Eq. (2.69). The modified eigenvalue problem that is to be solved is analogous to (1.55).

2.4 Results

The developed formalism is again applied to the α-α and n-α case, but this time in the microscopic FMD model. Resonance properties and phase shifts are calculated and compared to cluster models in the literature and experimental data.

2.4.1 Asymptotic Coulomb waves in ^{8}Be

Volkov No1 interaction

In order to test the collective-coordinate representation method, we compare its results with those of the calculation performed by Arai and Kruppa [16] using the same interaction and many-body state parameterization. The effective interaction is Volkov No. 1 with Majorana parameter $m = 6$ and the oscillator parameter is $\nu_\alpha = 0.235$ fm^{-2}. Since the width of the relative motion is $a_r = a/\mu_A$, where $a = 1/(2\nu_\alpha)$ is the width of the single particle states, the separation between neighbouring states is $\Delta_g = 1$ fm $\approx \sqrt{a_r}$. The closest configuration is at $D = 1$ fm.

Table (2.1) displays the good agreement between the different approaches. As the collective-coordinate representation also allows for a discrete representation of the wave function of the relative motion, we show in Fig. (2.1) the Gamov wave function for the $J^\pi = 0^+$ resonance.

The phase shifts for elastic scattering are depicted in Fig. (2.2). The energy range that can be covered is limited by the basis. The reason for this is that the width of the relative wave-packet cannot be chosen but depends on the widths of the cluster states. In the cluster model, where all gaussians have the same width parameter, the total center of

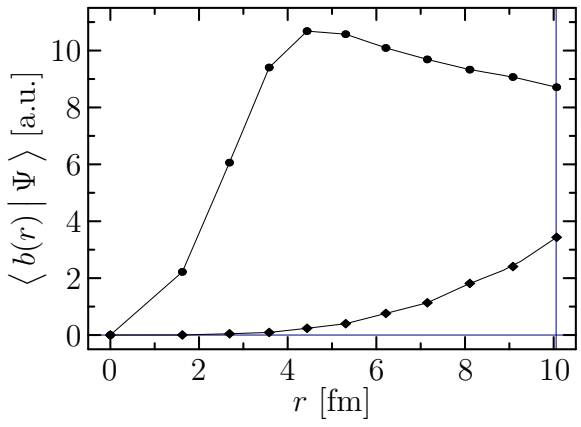

Figure 2.1: Real (circles) and imaginary (diamonds) parts of the Gamov wave function for the relative motion in the collective-coordinate representation, for the ^{8}Be $J^\pi = 0^+$ resonance.

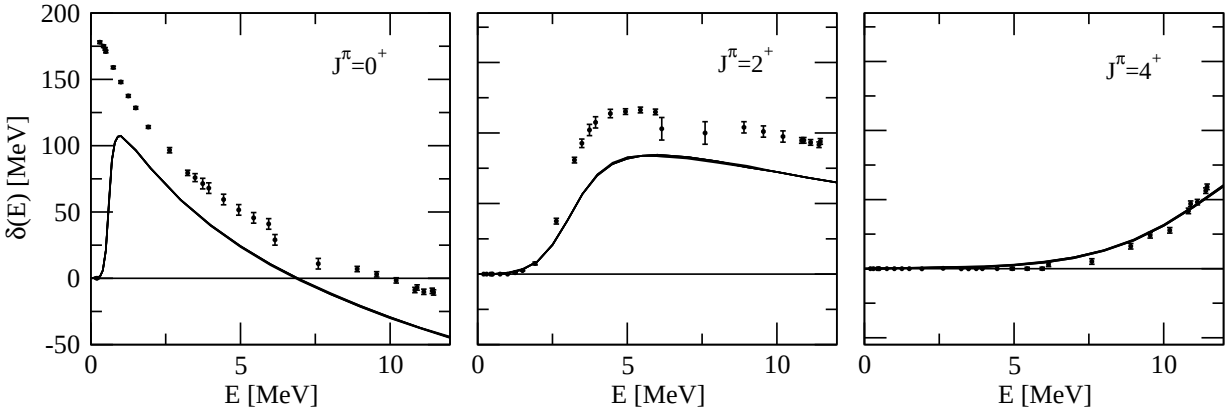

Figure 2.2: α-α phase shifts for $J^\pi = 0^+,\ 2^+,\ 4^+$ and Volkov No. 1 interaction obtained with the collective-coordinate representation by imposing scattering boundary conditions. Curves for several matching points ($r(b_t)$ =9.1, 10.0, 11.0, 12.0, 13.0) and comparison with the experimental points [17, 18, 19].

mass and the relative motion can be factorized. The gaussian of the relative coordinate is μ_A times more narrow ($\mu_A = 2$ for the α-α case) than the single-particle gaussian. As we have seen in the schematic model, this width parameter limits the representation of the relative motion to low energy, for which the wave function has small enough curvature. Future research should include in the basis (2.24), states in which the clusters have relative momentum besides the static states in which the clusters are at rest. This should allow the model to be extended to higher energies.

Although the phase shift calculation for $J^\pi = 4^+$ is performed only up to 12 MeV, the resonance at 11.6 MeV is obtained with the corresponding width using the purely outgoing boundary condition, or Gamov state. Note how the different curves, for several matching points, develop a narrow band, showing the limitations of the model space. This effect is more noticeable for the ^{5}He case discussed in the next subsection.

AV18-based interaction

Using the Unitary Correlation Operator Method (UCOM), Feldmeier, Neff and Roth [13, 20] have derived a low momentum interaction based on the realistic AV18 interaction. Augmented by small phenomenological corrections, many bound state properties of nuclei up to $A = 48$ have been described successfully in the framework of FMD [21, 22, 23]. In the following application we use this NN interaction to describe the ^{8}Be nucleus. It should be noted that, in contrast to all other interactions used, this interaction is not adjusted to fit the data of the system under consideration.

		$J^\pi = 0^+$		$J^\pi = 2^+$		$J^\pi = 4^+$	
		E [MeV]	Γ [MeV]	E [MeV]	Γ [MeV]	E [MeV]	Γ [MeV]
	Experiment	0.09204(5)	5.57(25) [eV]	3.12(1)	1.513(15)	11.44(15)	≈ 3.5
Volkov	CLD [16]	0.60	0.25	3.07	2.38	11.60	6.99
	CSM [16]	0.59	0.24	3.07	2.39	11.60	7.04
	Phase Shift [16]	0.60	0.25	3.07	2.38	11.60	7.00
	FMD	0.59	0.25	3.08	2.39	11.59	6.94
AV18-based	FMD	0.273(3)	0.0130(5)	2.71(2)	2.38(2)	-	-

Table 2.1: Resonance parameters for the α-α system using the Volkov and AV18-based interactions. Results are shown from the present work (FMD) and comparisons made to previous calculations. Experimental results are taken from [9]. Errors on calculated values denote uncertainty due to different matching points.

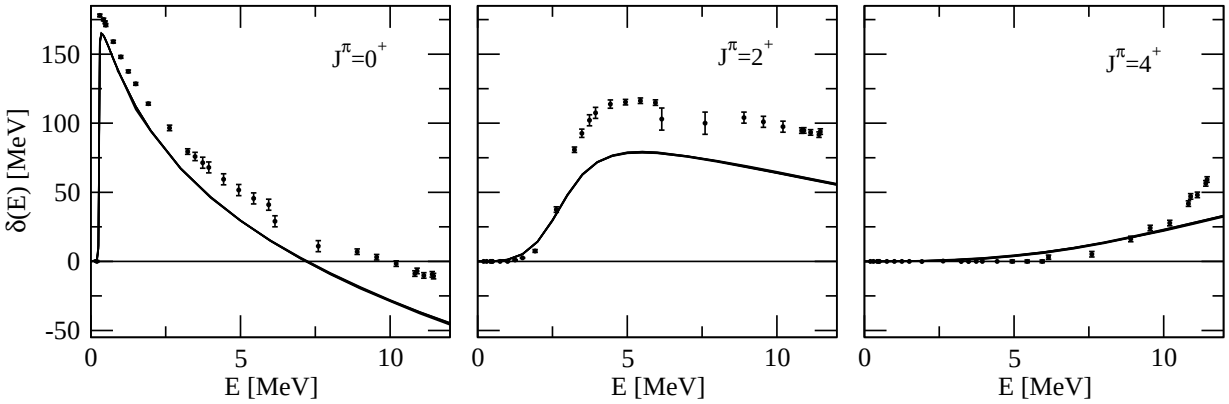

Figure 2.3: α-α phase shifts for $J^\pi = 0^+, 2^+, 4^+$ and AV18-based interaction obtained with the collective-coordinate representation by imposing scattering boundary conditions. Curves for several matching points ($r(b_t)$ =8.1, 9.0, 10.0, 11.0) and comparison with the experimental points [17, 18, 19].

The α-cluster is represented by the most simple mean-field ground state of ^{4}He, with just one gaussian per particle. The different intrinsic configurations that span the model space consist of two α-clusters at various relative distances (frozen state approximation). The states are chosen as previously.

The results for the resonances are shown in Table (2.1). We observe that the result for the 0^+ resonance is improved, getting closer to the experimental one. But one should bear in mind that resonance energy and width are correlated and a very precise reproduction of the experimental binding energy of ^{4}He is needed. The phase shifts depicted in Fig. (2.3) show the correlation between the resonances and the phase shifts. Since the 0^+ resonance is better reproduced with this interaction, also the phase shifts lie closer to the experimental ones, while the 2^+ are as bad. The 2^+ resonance lies 0.4 MeV too low for the AV18-based interaction, and the 4^+ partial wave does not show a resonance at all within the model space.

In summary, it seems that the AV18-based interaction leads to a looser barrier in the α-α potential compared to the phenomenological nucleus-nucleus potentials that are fitted to the scattering data.

2.4.2 Loosely bound neutron in ^{5}He

^{5}He is chosen again as a resonance without Coulomb interaction between the fragments. The calculation is done with both a phenomenological interaction describing the n-α phase shifts and then with the AV18-based interaction based on a realistic interaction. The former allows us to test the validity and accuracy of the result by comparing it to the same observables obtained by other approaches, whilst the latter, together with the aforementioned ^{8}Be calculations, provide the first results in FMD using a realistic interaction.

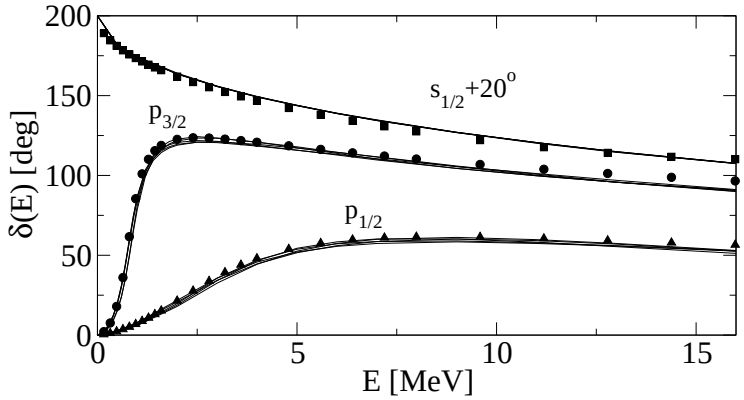

Figure 2.4: Phase shifts for ^{5}He calculated using a Minnesota potential in a frozen n-α configuration for several matching points ($r(b_t)$ =7.6, 9.1, 10.6, 12.1 and 13.5 fm). Dots, squares and triangles depict the experimental points [24] (the error bars are smaller than the dot size).

Minnesota interaction with Reichstein-Tang spin-orbit

The effective NN force is the Minnesota potential including a Reichstein-Tang spin-orbit force (set No. IV, see [16] and references therein). The oscillator parameter is ν_α = 0.303 fm^{-2}. The basis states are chosen in order to ensure the coverage of the Hilbert space in an optimal way, following the previous reasoning: the separation between neighbouring

		$J^\pi = 3/2^-$		$J^\pi = 1/2^-$	
		E [MeV]	Γ [MeV]	E [MeV]	Γ [MeV]
	Experiment	0.798	0.648	2.07	5.57
Minnesota	CLD [16]	0.78	0.64	2.01	5.42
	Phase Shift[16]	0.78	0.64	1.98	5.45
	S-Matrix, RGM [25]	0.76	0.63	1.89	5.20
	FMD	0.82(4)	0.73(8)	1.98(28)	5.44(30)
AV18-based	FMD	0.36(1)	0.23(1)	1.52(19)	4.92(25)

Table 2.2: Resonance parameters for the n-α system using the different interactions. Results are shown from the present work (FMD) and comparisons made to previous calculations. Experimental results are taken from [5]. Errors on calculated values denote uncertainty due to different matching points.

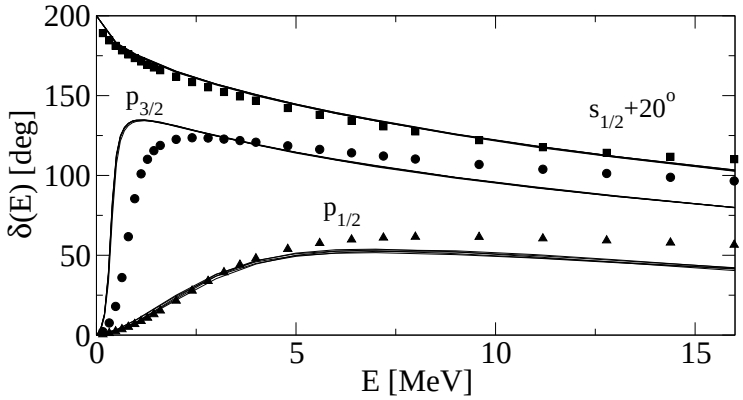

Figure 2.5: Phase shifts for ^{5}He calculated using an AV18-based potential in a frozen n-α configuration for several matching points ($r(b_t)$ =7.6, 9.1, 10.6, 12.1 and 13.6 fm). Dots, squares and triangles depict the experimental points [24] (the error bars are smaller than the dot size).

states is $\Delta_g = 1.5$ fm $\approx \sqrt{a}$ and the closest configuration is at $D = 1.5$ fm relative distance.

The agreement with the results given by Arai and Kruppa [16] is not as good as in the ^{8}Be case (see Tab. (2.2)). Only taking into account the uncertainties due to the angular momentum projection can already affect the result by 0.01 MeV. Moreover, these are wide resonances and thus are less suited to the Gamov vector approximation. Note that the Gamov results are always slightly higher than those of other approaches. This was also the case in the schematic model, where phase shift analysis and eigenvalues of Gamov vectors did not yield exactly the same result.

Phase shifts are depicted in Fig. (2.4) for different matching points. Recalling that the interaction is fitted to the experimental phase shifts of n-α elastic scattering, the agreement with the experiment confirms the validity of our method.

AV18-based interaction

The α-cluster is the same as in the ^{8}Be case with this interaction. The extra neutron is given the same width as those in the cluster. The different configurations are again chosen to be frozen states as in Eq. (2.24). The separation and distribution of the states along the reaction path is the same as in the previous case, since $a = 1.78$ fm^2 and thus $\Delta_g = 1.5$ fm again. A few configurations are displayed in Fig. (1), in the introduction.

The results, displayed in Table (2.2), do not describe the resonances as well as the dedicated models where the parameters of the NN-interaction have been adjusted to fit the reaction under consideration. The main difference to the measured values is the energy position with respect to ^{4}He, the calculated values are about 0.44 MeV lower than the measured ones. Here one has to keep in mind that the ground state of ^{4}He moves down about 0.5 MeV when two gaussians per particle are used. Thus, it is quite conceivable that

a better starting point for the ^{4}He fragment will improve the agreement. The spin-orbit splitting is well reproduced.

For energies above 2.5 MeV the phase shifts reproduce the experimental ones for the s-wave, while the p-wave results appear distorted since the resonances are not reproduced at the right position. Thus we can conclude that the AV18-based interaction describes the phase shifts qualitatively, but one has to keep in mind that no free parameters have been specifically adjusted and only simplistic many-body states are used. The agreement is surprising because high precision is needed in order to accurately describe the experimental results, the binding energies of ^{4}He and ^{5}He must agree with the experimental ones to an accuracy of less than a 1%. Being less ambitious, one could also set the energy threshold such that it corresponds to the experimental one. In that case, the phase shifts and resonances are shifted in energy and thus might also better reproduce the experimental results.

Summary and Outlook

We have developed a method to implement boundary conditions in nuclear many-body microscopic models by means of a collective-coordinate representation. This method requires only the definition of asymptotic channel states with separate fragments, leaving complete freedom to the configuration of the system when the fragments are close to each other. Hence, it allows the investigation of scattering and resonant states.

The collective-coordinate representation is the keystone for the formulation of the boundary conditions in the many-body Hilbert space. It can be obtained from a microscopic representation of the nuclear system, in which the nucleons are the fundamental components. The physical interpretation of the collective coordinate as the relative distance between the fragments is, by construction, unique in the asymptotic region, but it can also be used for the interior region where the two clusters are close to each other and their components are indistinguishable. This representation allows the relative distance between the clusters to be defined in terms of valid observables for antisymmetrized systems. Moreover, a wave function of the system in this representation can be defined, as well as its derivatives. The formalism is written in terms of operators and states defined in a model Hilbert space, which is spanned by the set of many-body states that build the reaction path.

Several tests have been conducted in schematic models for both free spherical and Coulomb asymptotic waves. These help to visualize the nature of the method, and also to extend its application towards a fully antisymmetrized microscopic many-body problem with a nonorthogonal basis of extended but localized states.

First results are presented in the framework of Fermionic Molecular Dynamics (FMD). Comparison to results previously obtained, using the same many-body parameterization and interaction, confirm the validity and show the accuracy of the method; whilst its application to ^{5}He employing a realistic interaction agrees with experiment apart from the fact that the α-particle is somewhat underbound in the simplified model space used in this work. This is very promising since there are no free parameters that have to be adjusted to the n-α system. It shows that this microscopic NN force is able to describe resonances and phase shifts at least qualitatively, and at times accurately. In short, the present work extends the application of the FMD model to continuum states.

The first step to further improve the results would be the choice of better basis states. In order to treat scattering states at higher energy, the basis states could also include states with a relative momentum between the fragments. For a better description of the interior

region, polarization effects might be included, minimizing the energy whilst keeping the distance between the clusters constant.

More elaborate single-particle states are needed for some systems. For example, the use of two gaussians per nucleon yields an improved description of the fragments.

Coupled channel calculations and reactions of the type A(a,b)B may also be tackled with an extension of this method. Finally, the collective-coordinate representation may be used in future applications to derive effective nucleus-nucleus potentials.

Bibliography

[1] C. Cohen-Tannoudji et al., *Quantum Mechanics*, John Wiley & Sons, 1997.

[2] A. Bohm, *Quantum Mechanics: Foundations and Applications*, Springer Verlag, third edition, 1994.

[3] G. Gamow, *Zur Quantentheorie des Atomkernes*, Z. Phys. 51 (1928) 510

[4] G. R. Satchler et al., *An optical model for the scattering of nucleons from* ^{4}He *at energies below 20 MeV*, Nuc. Phys. A112 (1968) 1-31.

[5] D. R. Tilley et al., *Energy levels of light nuclei A=5*, Nucl. Phys. A708 (2002) 3.

[6] S. Ali and A. R. Bodmer, *Phenomenological α-α potentials*, Nuc. Phys. 80 (1966) 99-112.

[7] I. J. Thompson, A. R. Barnett, CERN Program Library Short Writeup CCLBES(C309), 1988 (Revised 1995).

[8] L. Landau and E. M. Lifshitz, *Quantum Mechanics (Non-relativistic Theory)*, Pergamon Press, third edition, 1977 (Reprint 1981).

[9] D. R. Tilley et al., *Energy levels of light nuclei A=8*, Nucl. Phys. A745 (2004) 155.

[10] J. P. Blaizot and G. Ripka, *Quantum Theory of Finite Systems*, The MIT Press, 1986

[11] H. Feldmeier, J. Schnack, *Fermionic Molecular Dynamics*, Prog. Part. Nucl. Phys. 39 (1997) 393-442

[12] R. Machleidt, F. Sammarruca, and Y. Song, *Nonlocal nature of the nuclear force and its impact on nuclear structure*, Phys. Rev. C, 53 (1996) 1483

[13] T. Neff and H. Feldmeier, *Tensor correlations in the unitary correlation operator method*, Nuc. Phys. A713 (2003) 311

[14] T. Neff, H. Feldmeier, R. Roth, J. Schnack, *Realistic Interactions and Configuration Mixing in Fermionic Molecular Dynamics*, Proc. of the International Workshop XXVII on Gross Properties of Nuclei and Nuclear Excitations, Hirschegg, Austria, January 17-23, 1999 (xxx-Preprint nucl-th/9902049)

[15] D. A. Varshalovich, A. N. Moskalev and V.K. Khersonskii, *Quantum Theory of Angular Momentum*, World Scientific Publishing Co Pte Ltd., 1988

[16] K. Arai and A. T. Kruppa, *Continuum level density in a microscopic cluster model: Parameters of resonances*, Phys. Rev. C 60 (1999) 064315

[17] N. P. Heydenburg and G. M. Temmer, *Alpha-alpha Scattering at Low Energies*, Phys. Rev. 104 (1956) 123

[18] T. A. Tombrello and L. S. Senhouse, *Elastic Scattering of Alpha Particles from Helium*, Phys. Rev. 129 (1963) 2252

[19] R. Nilson et al, *Investigation of Excited States in* ^{8}Be *by Alpha-Particle Scattering from He*, Phys. Rev. 109 (1958) 850

[20] R. Roth, T. Neff, H. Hergert, H. Feldmeier, *Nuclear Structure based on Correlated Realistic Nucleon-Nucleon Potentials*, Nucl. Phys. A745 (2004) 3

[21] T. Neff, H. Feldmeier, *Cluster Structures within Fermionic Molecular Dynamics*, Nucl. Phys. A738 (2004) 357

[22] T. Neff, H. Feldmeier and R. Roth, *Structure of light nuclei in Fermionic Molecular Dynamics*, Proc. of the International Nuclear Physics Conference 2004, Gteborg, Sweden (to appear in Nucl. Phys. A)

[23] T. Neff, H. Feldmeier and R. Roth, *Cluster and Shell-Structure in Light Nuclei*, Proc. of the Nuclei at the Limits Conference 2004, Argonne National Lab, USA (to appear in AIM proceedings)

[24] J. E. Bond and F. W. K. Firk, *Determination of R-function and physical-state parameters for n-*^{4}He *elastic scattering below 21 MeV*, Nucl. Phys. A 287 (1977) 317

[25] A. Csótó and G. M. Hale, *S-Matrix and R-Matrix determination of the low-energy* ^{5}He *and* ^{5}Li *resonance parameters*, Phys. Rev. C55 (1997) 536

Curriculum Vitae

Personal Data

Name	Alberto
Surname	Cribeiro Santalla
Place of Birth	Cedeira (A Coruña)
Date of Birth	11 January 1979
Marital Status	single
Nationality	spanish

Education

09 / 1985 - 06 / 1993	EGB (Primary School), C.P. O Feal, Narón Sobresaliente (excellent)
09 / 1993 - 06 / 1997	BUP&COU (Secondary School), I.E.S. Terra de Trasancos, Narón. MdeH (excellent with distinction)
06 / 1997	Selectividad (university entrance examination), 8.24 over 10
09 / 1997 - 06 / 2001	Licenciado en Físicas (graduate in Physics), Santiago de Compostela. Main subject Particle Physics. Average grade 2.7 (very good)
01 / 2002 - 05 / 2005	Doctoral fellowship at the Gesellschaft für Schwerionenforschung and preparation of the dissertation

Acknowledgements

I am sincerely indebted to Prof. Dr. Hans Feldmeier for the opportunity to join his group. He patiently taught me how to think scientifically, the process to follow in order to do research and to express and understand complicated concepts by means of intuitive examples. He also helped me to give a formal shape to the ideas that were coming into my mind and that I could not put onto paper in the form of equations, thereby filling the gaps of my always incomplete training. I only hope that I will always bear his advice in mind. The title *Doktorvater* accurately summarizes what he has represented during these years, his guidance going further than the academic and professional boundaries, entering aspects of life that have helped me to grow as a person, and providing advice and help in matters that appeared quite difficult upon arriving in a foreign country.

Dr. Thomas Neff deserves a special mention, since he was the patient man who was always there when I cried "help!", whenever I found one of the many problems, providing a critical point of view that sometimes caused me to despair, but more importantly helped me to do my best.

Discussions with both Prof. Dr. Hans Feldmeier and Dr. Thomas Neff have been and will surely continue to be very fruitful, they have also been the source of all ideas displayed here.

Thanks to GSI, in particular to Prof. Dr. Wolfgang Nörenberg and the GSI theory group, for the fellowship they have granted me and for giving me the opportunity to get involved in the real day-to-day business of research. I should also mention here the GSI International Summer Student Program and the organizers Jörn Knoll and Heide Rinnert, since they enabled me to come here for the first time. Prof. Dr. Robert Roth was outstanding as my direct supervisor and made me feel comfortable as one more member of the crew. The program continues to make a nice noise here each summer.

I am very grateful to Rob Cussons, not just because he is a native English speaker with lots of patience, but because he is a real friend. Isaac Vidaña and Matthias Möller are preparing what will surely be an outstanding buffet that will mark a turning point; I thank them in advance for this, but more importantly for many other reasons.

To all my friends I apologize because I have not made a lengthy list of all of you, but you know I keep you in my thoughts. I thank the ones I left in Galicia and are still there, who supported me even when I was leaving them and continue to do so; but also the ones I have made here, who fascinated me with their countries and cultures, so different from my own but the same at heart. Thank you all for the great moments and for listening when I needed you.

Thank you Paola for sharing these years and especially for your support in the hardest final moments, while I write these words.

Finally, it is not possible to express how grateful I am to my family, who have been enduring my absence and worrying about me everyday. Even so, they are happy for me and continue to take care of me, despite the distance, with good words and advice.

Papá, gracias por manterte sempre en contacto e pola túa insistencia machacona. Mamá, gracias por terme tanta paciencia e comprensión.

Erklärung

Hiermit erkläre ich an Eides statt, daß ich die vorliegende Dissertation selbständig verfaßt, keine anderen als die angegebenen Hilfsmittel verwendet und noch keinen Promotionsversuch unternommen habe.

Darmstadt, den 24. Mai 2005,

gez. Alberto Cribeiro Santalla.

Unterschrift